Luís Filipe Madureira Fonseca

Licenciado em Bioquímica

Bioremediation and CO_2 scavenging using molybdenum-containing enzymes

Dissertação para obtenção do Grau de Mestre em Bioquímica

Orientadores: José João Galhardas de Moura, Professor Catedrático, Faculdade de Ciências e Tecnologia da Universidade Nova de Lisboa

Isabel Maria Andrade Martins Galhardas de Moura, Professora Catedrática, Faculdade de Ciências e Tecnologia da Universidade Nova de Lisboa

Co-orientadora: Luísa Bernardina Lopes Maia, Investigadora Pós-Doc, Faculdade de Ciências e Tecnologia da Universidade Nova de Lisboa

Júri:

Presidente: José Ricardo Ramos Franco Tavares

Arguente: Stéphane Pierre Bensson

Vogal: José João Galhardas de Moura

FACULDADE DE CIÊNCIAS E TECNOLOGIA
UNIVERSIDADE NOVA DE LISBOA

Outubro, 2014

Luís Filipe Madureira Fonseca

Licenciado em Bioquímica

Bioremediation and CO_2 scavenging using molybdenum-containing enzymes

Dissertação para obtenção do Grau de Mestre em Bioquímica

Orientadores: José João Galhardas de Moura, Professor Catedrático, Faculdade de Ciências e Tecnologia da Universidade Nova de Lisboa

Isabel Maria Andrade Martins Galhardas de Moura, Professora Catedrática, Faculdade de Ciências e Tecnologia da Universidade Nova de Lisboa

Co-orientadora: Luísa Bernardina Lopes Maia, Investigadora Pós-Doc, Faculdade de Ciências e Tecnologia da Universidade Nova de Lisboa

Júri:

Presidente: José Ricardo Ramos Franco Tavares

Arguentes: Stéphane Pierre Bensson

Vogais: José João Galhardas de Moura

Outubro, 2014

Bioremediation and CO_2 scavenging using molybdenum-containing enzymes.

Para os meus avós

AGRADECIMENTOS

O trabalho desenvolvido no âmbito desta dissertação, apenas foi possível devido à contribuição de diversas pessoas a quem gostaria de expressar os meus agradecimentos.

Em primeiro lugar, gostaria de agradecer aos meus orientadores Prof. José J. G. Moura e Prof.ª Isabel Moura, por me terem aceite nos seus grupos de investigação e por me proporcionarem todas as condições necessárias para a realização deste trabalho.

Um agradecimento à Doutora Luísa Maia, por ter orientado de perto esta dissertação, pela sua paciência e por me ter transmitido conhecimentos que em muito contribuíram para ampliar a minha formação científica.

Aos meus colegas, Francisco, Joana e Lara um agradecimento pela amizade, companheirismo e entreajuda que sempre existiu ao longo da preparação desta dissertação e, pelas animadas conversas que sempre ajudaram a desanuviar nos dias em que "a ciência" corria menos bem.

Uma palavra de agradecimento também à Célia Silveira, pelas frutuosas conversas e discussões científicas e por toda a ajuda, quer com os crescimentos bacterianos, quer na preparação dos ensaios cinéticos.

Gostaria também de demonstrar a minha gratidão a todos os membros dos grupos *BioIn* e *Bioprot* pelo excelente acolhimento. Em particular, à Cíntia Carreira, Cláudia Nóbrega e Rute Nunes pela ajuda, disponibilidade e conselhos.

Não posso deixar de agradecer à técnica dos laboratórios 407 e 617, Ana Teresa Lopes, pela constante disponibilidade e ajuda; nem olvidar um agradecimento especial às técnicas do 4º piso: Idalina Martins e Maria da Conceição Luís por tornarem o meu trabalho no laboratório mais fácil.

E porque o que somos é o resultado de uma mistura de experiências e ensinamentos que vamos adquirindo ao longo das nossas vivências, quero deixar um agradecimento a todas as "peças" do infinito "puzzle" que é a minha vida, que nunca me deixaram desistir ou deixaram de acreditar em mim.

Aos meus amigos Ana, Diana, Ivo, João, Miguel, Raquel, Ricardo, Teresa,

agradeço o facto de, independentemente da distância, terem estado sempre presentes, inclusivamente quando eu não podia estar!…

Rute, obrigado por teres estado presente nos momentos menos bons, por teres tornado menos trabalhosa a escrita desta tese e por me teres mostrado que com paciência e dedicação tudo é possível.

A toda a minha família, (aos que estão e aos que já não podem assistir…) tenho a agradecer o apoio incondicional, força, incentivo e amizade sem igual. Aos meus pais e à minha irmã um incomensurável agradecimento por tudo o que têm feito por mim afinal, tal como não podemos almejar voar se nos cortarem as asas, nunca haverá palavras que expressem a minha profunda gratidão. Sem todos vós nada disto seria possível.

ABSTRACT

Carbon dioxide valorization, will not only help to relieve the greenhouse effect but might also allow us to transform it in value-added chemicals that will help overcoming the energy crisis. To accomplish this goal, more research that focus on sequestering CO_2 and endeavors through a carbon-neutral or carbon-negative strategy is needed in order to handle with the dwindling fossil fuel supplies and their environmental impact. Formate dehydrogenases are a promising means of turning CO_2 into a biofuel that will allow for a reduction of greenhouse gas emissions and for a significant change to the economic paramount. The main objective of this work was to assess whether a NAD^+-independent molybdenum-containing formate dehydrogenase is able to catalyze the reduction of CO_2 to formate. To achieve this, a molybdenum-containing formate dehydrogenase was isolated from the sulfate reducing bacteria *Desulfovibrio desulfuricans* ATCC 27774. Growth conditions were found that allowed for a greater cellular mass recovery and formate dehydrogenase expression. After growth trials, kinetic assays for formate oxidation and CO_2 reduction were performed and kinetic parameters determined. For the formate oxidation reaction, a K_M of 49 μM and a turnover constant of 146 s^{-1} were determined. These kinetic parameters are in agreement with those determined by Mota, *et al*. (2011). Finally, we found that this molybdenum-containing enzyme was able to catalyze the reduction of CO_2 to formate with a turnover constant of 4.6 s^{-1} and a K_M of 13 μM. For the first time a NAD^+-independent molybdenum-containing formate dehydrogenase was found to catalyze CO_2 reduction, allowing its use as a biocatalyst in energetically efficient CO_2 fixation processes that can be directed towards bioremediation or as an alternative and renewable energy source. Characterizing these enzymes may lead to the development of more efficient synthetic catalysts, make them readily available and more suited for practical applications.

Keywords: formate dehydrogenase; molybdoenzymes; CO_2 reduction; bioremediation.

RESUMO

A valorização do CO_2, através da sua conversão em produtos de valor acrescentado, não só é importante para diminuir o efeito de estufa mas também para obter biocombustíveis que nos podem auxiliar a ultrapassar a crise energética. Para atingir este objectivo, é necessário focar a investigação no sequestro de CO_2 e na sua valorização, de modo a lidar com a crescente escassez de combustíveis fósseis e com o impacto ambiental que a sua utilização acarreta. As formato desidrogenases são um meio promissor para transformar CO_2 num biocombustível que permitirá, além da redução das emissões de gases com efeito de estufa, operar uma alteração significativa no contexto económico. O principal objectivo deste trabalho foi determinar se uma formato desidrogenase contendo molibdénio e independente de NAD^+, é capaz de catalisar a redução de CO_2 a formato. Para tal, foi isolada uma formato desidrogenase da bactéria redutora de sulfato *Desulfovibrio desulfuricans* ATCC 27774. Foram encontradas as condições de crescimento bacteriano que permitiam, simultaneamente, uma maior recuperação de massa celular e de expressão da enzima. Seguidamente, caracterizou-se cineticamente a reacção de oxidação de formato a CO_2 tendo-se determinado um K_M para o formato de 49 μM e uma constante catalítica de 146 s^{-1}. Os parâmetros cinéticos para esta reacção, estão de acordo com os que foram obtidos por Mota, *et al*. (2011). Finalmente, verificou-se que esta enzima é capaz de catalisar a redução de CO_2 com uma constante catalítica de 4.6 s^{-1} e um K_M de 13 μM. Permitindo, pela primeira vez, demonstrar que uma formato desidrogenase independente de NAD^+ e contendo molibdénio, é capaz de catalisar a redução de dióxido de carbono a formato possibilitando a sua utilização como biocatalisador energicamente eficiente na fixação de CO_2, a sua aplicação em processos de bioremediação ou como uma fonte de energia alternativa e renovável. Caracterizar estas enzimas torna possível o desenvolvimento de catalisadores sintéticos mais eficientes, facilmente disponíveis e mais adequados a aplicações práticas.

Palavras-chave: formato desidrogenase; enzimas de molibdénio; redução de CO_2; bio-remediação.

TABLE OF CONTENTS

FIGURES INDEX

TABLE INDEX

ABBREVIATIONS

Asp	Aspartate
ATCC	American type culture collection
β-ME	Beta-mercaptoethanol
BV	Benzyl viologen
COdh	Carbon monoxide dehydrogenase
Cys	Cysteine
D. desulfuricans or *Dd*	*Desulfovibrio desulfuricans* ATCC 27774
D. gigas or *Dg*	*Desulfovibrio gigas*
D. vulgaris or *Dv*	*Desulfovibrio vulgaris*
DMSO	Dimethyl sulfoxide
DMSOr	Dimethyl sulfoxide reductase
DTT	Dithiothreitol
ε	UV-Visible molar extinction coefficient
E. coli	*Escherichia coli*
EDTA	Ethylenediaminetetraacetic acid
Fdh	Formate dehydrogenase
GHG	Greenhouse effect gas
HPLC	High-performance liquid chromatography
KPB	Potassium phosphate buffer
Moco	Molybdenum cofactor
Mo-enzymes	Molybdenum-containing enzymes
Mo/W-enzymes	Molybdenum/Tungsten-containing enzymes

MV	Methyl viologen
NAD^+	Nicotinamide adenine dinucleotide oxidized form
NADH	Nicotinamide adenine dinucleotide reduced form
O.D.	Optical density
PAGE	Polyacrylamide gel electrophoresis
PCD	Pyranopterin cytosine dinucleotide
PGD	Pyranopterin guanine dinucleotide
PMP	Pyranopterin monophosphate
PMSF	Phenylmethylsulfonyl fluoride
RMSD	Root mean square deviation
SDS	Sodium dodecyl sulfate
SeCys	Selenocysteine
So	Sulfite oxidase
Ser	Serine
SRB	Sulfate reducing bacteria
UV-Vis	Ultraviolet-Visible
W-enzymes	Tungsten-containing enzymes
Xo	Xanthine oxidase

I. INTRODUCTION

I. INTRODUCTION

Two major energy-related issues will daunt the world in the next fifty years. On one hand, nations will progressively have to dispute access to fossil fuels as reserves gradually become scarce, leading to an energy cost increase. On the other hand, atmospheric carbon dioxide (CO_2) levels are at their highest level since recording of its concentrations in the atmosphere began. The predictions show that large increases in its concentration will probably produce large and uncontrollable changes on world climate. Figure I.1 shows that CO_2 accounts for more than half of global greenhouse effect gases (GHG) emitted to the atmosphere, and that its main source are the fossil fuels we use in our daily lives. Therefore, it is important to develop new energy sources that are both secure and carbon neutral.

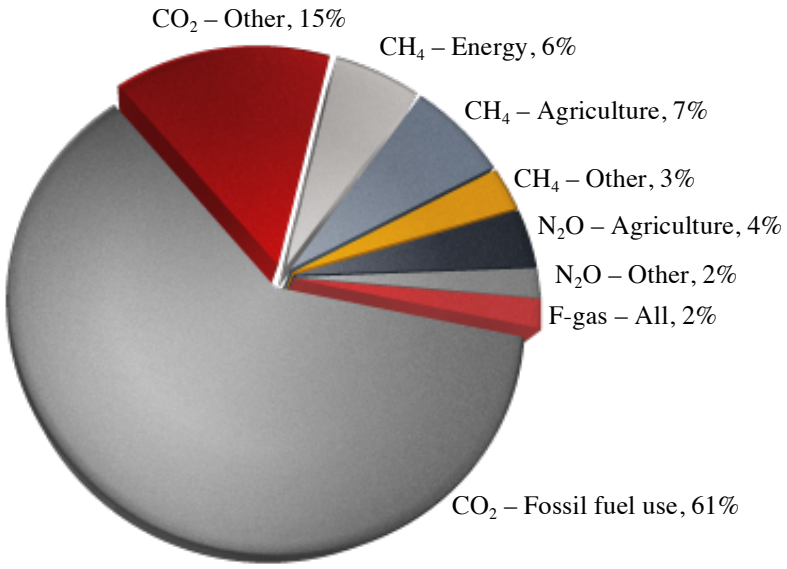

Figure I.1 – Global GHG emissions for 2010. Adapted from [1].

I.1. Carbon dioxide

Carbon dioxide is a trace gas in the atmosphere of the Earth. And although it represents only 0.04% (400ppm) of the gases that constitute the atmosphere it is a potent GHG and plays a critical role in the regulation of the climate on Earth. Hence, keeping its concentration within a certain range is a crucial factor to prevent further changes to the current climate pattern.

Ever since the beginning of the Industrial Revolution around 150 years ago, the amount of CO_2 in the atmosphere has increased noticeably, from 280 to about 400 ppm this year, and keeps increasing at a rate of about 1.9 ppm/year (Figure I.2).

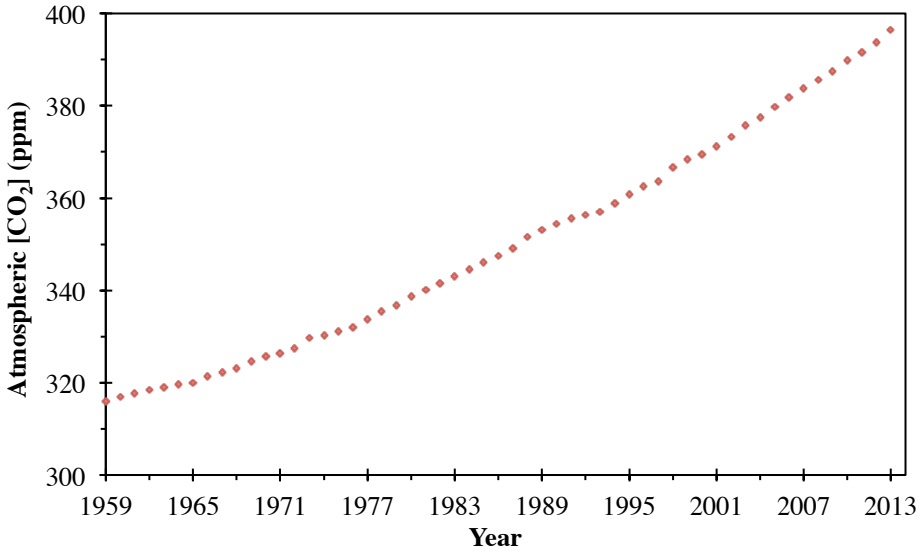

Figure I.2 – Atmospheric carbon dioxide concentrations, in ppm, since record began at Mauna Loa Observatory in 1958 [2]**.**

This increase is linked to the burning of fossil fuels resulting from human activities and has the potential to induce climate change, making this phenomenon one of global concern [3–5]. According to the Third Assessment Report (2001) of the Intergovernmental Panel on climate change an increase in the GHG levels could lead to a temperature raise which, in turn, could have an impact on global climate patterns.

Nowadays, there is global awareness to the depletion of fossil fuel reserves and to the generally accepted fact that their consumption has caused increasing anthropogenic

GHG emissions. Thus, it is important that we rapidly adapt and procure new primary energy sources that allow us, in the long run, to completely replace fossil fuels. To achieve this goal, it is necessary to develop novel carbon abatement techniques and mature those we are experimenting on, while evolving policies to promote renewable energy sources that enable us to sequester atmospheric greenhouse gases such as CO_2. As depicted in Figure I.3, the majority of the GHG released into the atmosphere are resultant from energy production processes, and CO_2 is the main GHG being released into the atmosphere, making it an important candidate for these carbon capture techniques.

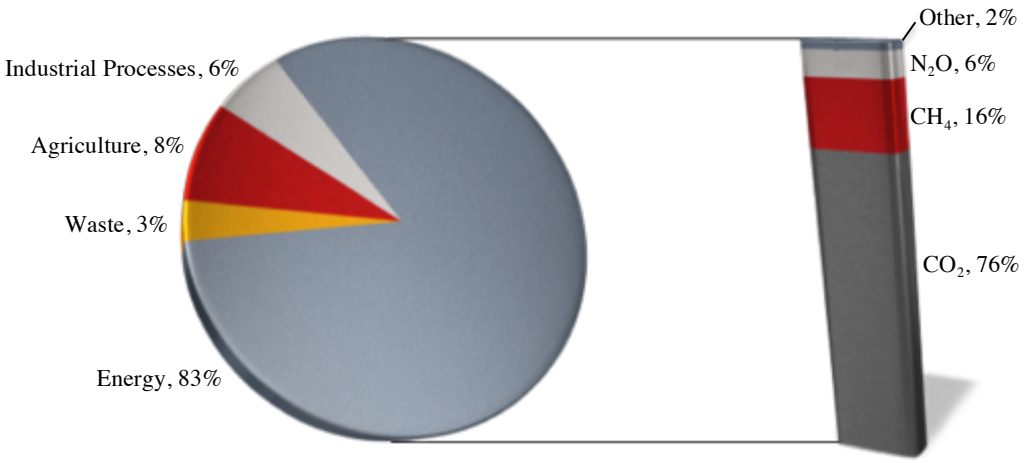

Figure I.3 – Global GHG emissions for 2013 by source and type. Adapted from [6].

Although it is impossible to capture all the CO_2 produced daily, it is still crucial to make an effort to mitigate the consequences its increase in the atmosphere may have to future generation. CO_2 capture can be achieved in two ways: straight from the atmosphere or directly from a source and it can either be converted into useful chemicals (Figure I.4) or sequestered (Figure I.5).

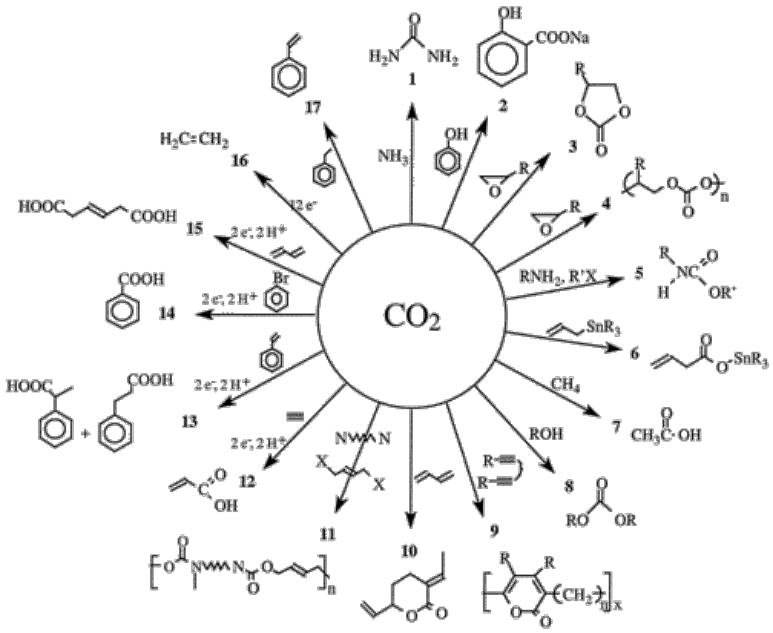

Figure I.4 – Possible chemical transformations of CO_2. Adapted from [7].

Figure I.5 – Carbon capture and storage facilities implemented throughout the World. Adapted from [8].

The main challenge in converting CO_2 into useful products, such as industrially important chemicals and fuels, is its thermodynamic stability. As a product of cellular respiration or fossil fuel burning, returning CO_2 to a useful state by activation/reduction

is still quite challenging since it requires a large energy input and suitable catalysts. The response to such a scientific challenge derives from several fields of knowledge, *i.e.*, chemical catalysis, photochemistry, electrochemistry and semiconductor physics and engineering [5].

Nonetheless, the possibility of recovering CO_2 directly from the atmosphere poses a serious challenge due to its concentration, and *in situ* capture technologies are yet to overcome the difficulties presented by the great amount of energy required to purify, transport and storage it [9,10]. The more traditional solutions, as the ones cited, also pose other drawbacks, such as low selectivity and non-specificity that lead to the production of mixtures [11].

In any case, although the capture of CO_2 for posterior activation and conversion to a biofuel is not a straightforward process, it poses a great opportunity for solving the problems of fossil fuel shortage and global warming. There are numerous advantages of using CO_2 as a fuel source, namely its unlimited availability, and the fact its production, as opposed to the biofuels we are currently depending on, is not dependent of arable land.

In order to seriously consider CO_2 as an alternative fuel source we need to find a way to outstrip these classical approaches and arrive at an efficient and selective way to reduce CO_2 that allows for a reduction on our dependency of fossil fuels while aiding to balance the economic and environmental sustainability.

I.2. Reduced carbon dioxide as a novel source of energy

In the last decade, a major effort has gone into the research of a novel carbon-neutral energy source, with the main goal being the capture and recycling of atmospheric CO_2. The main research focus is its reduction into various energy rich molecules, by taking advantage of sunlight using plants and algae [12]. However, there are major flaws in this approach, namely, the complex matrix from which the product of interest must be harvested and the need for large areas of land for cultivation. By far, the most common approach to the problem is the utilization of metal catalysts to reduce CO_2 through both heterogeneous and homogeneous reactions and although important

progresses have been made in this field, metal catalysis usually continues to require extreme conditions in terms of pressure and temperature, and suffers from by-product formation [13–15]. To try to overcome the disadvantages of this latter technique, researchers are now aiming at the development of high-efficient photo-catalysts. However, although selectivity was greatly improved, efficiency continues to fall short [16,17]. Another approach that has been gaining prominence is the application of electrochemistry in the conversion of CO_2 into biofuels and other molecules of commercial interest. Nonetheless, this is still a recent technology that needs to be improved before it can become viable. The main drawback, besides being energetically unfavorable, is the production of multiple end-products as a result of cross reactions [18]. According to a 2008 report of the North American Department of Defense, "The major obstacle preventing efficient conversion of carbon dioxide into energy-bearing products is the lack of catalysts..." [19]. This being the case, biocatalysts are now viewed as an attractive research focus, as they open the possibility to circumvent the drawbacks of the more classical approaches.

I.3. Enzymes: from bioremediation and chemicals to biofuels

The use of enzymes in bioremediation processes is nothing new. However, their utilization in energy production, or in the valorization of by-products resulting from human activities, is yet to be established at an industrial scale mainly due to their requirements for intricate growth conditions, such as strict anaerobicity and complex purification procedures [20].

In Nature all biological systems need to be able to produce energy from their surroundings in order to sustain metabolic processes that are crucial to life. Nonetheless, as life is very adaptable these systems had to evolve and adjust to diverse conditions. CO_2 fixation pathways have evolved for millions of years and in this process diverse mechanisms and enzymes have been fine-tuned to perform this task. Carboxylases and dehydrogenases are among the enzymes that are able to catalyze the fixation of CO_2.

Carboxylases allow the creation of new carbon-carbon bonds by introducing HCO_3^- or CO_2 into target molecules. It is estimated that more than 98% of all CO_2 that

undergoes the biological carbon cycle is fixated by carboxylases [21]. The predominant mechanism, employed by plants and many prokaryotes to fix CO_2 is the reductive pentose phosphate (Calvin-Benson-Bassham) cycle. The cycle is initiated with the carboxylation of a five-carbon sugar, 1,5-ribulose bisphosphate, by the enzyme ribulose bisphosphate carboxylase/oxygenase (RuBisCO) to form two molecules of 3-phosphoglycerate that latter undergoes a succession of interconversions to form a six-carbon sugar, fructose-1,6-bisphosphate. Globally, this cycle catalyzes the following reaction [22,23].

(Eq. I.1)

$$3CO_2 + 5H_2O + 6NADPH + 9ATP \rightarrow$$

$$\rightarrow \text{3-phosphoglyceraldehyde} + 6NADP + 9\ ADP + 8P_i$$

Nonetheless, other enzymatic CO_2 reduction reactions exist. In methanogenensis, an eight-electron reduction of CO_2 to methane is performed [24], and in the folate-dependent one-carbon metabolism, CO_2 is converted to methyltetrahydrofolate, which is a key component of the reductive acetyl-CoA pathway [25].

Dehydrogenases are amid the best catalysts found in Nature [26–30]. Among these, CO dehydrogenases (COdhs) and formate dehydrogenases (Fdhs) are of special interest for CO_2 fixation. COdhs can be divided into two groups. The first groups O_2-sensitive enzymes, found in obligatory anaerobes, with $[Fe_4S_4Ni]$ active sites. The other group encompasses all air-stable COdhs, found in anaerobes, that have an [MoSCu] active site. Fdhs are a heterogeneous group of enzymes that will be the focus of this work. These enzymes, found in both prokaryotes and eukaryotes catalyze the oxidation of formate to CO_2 and H^+. Aerobic organisms have, mainly, NAD^+-dependent formate dehydrogenases, while prokaryotes, being more adaptable and able to thrive in harsher environments, such as anoxic ones, need to resort to terminal electron acceptors other than molecular oxygen [31,32]. The substrate of these enzymes, formate is a significant intermediary in the energy metabolism in prokaryotes [33,34]. Biologically, it can be produced by the degradation of amino-acids, pyruvate, hypoxanthine, oxalate and l-(+)-tartaric acid [35,36]. Under anaerobic conditions, formate is produced from

pyruvate and acts as a major electron donor to an assortment of inducible respiratory pathways that rely on NAD^+-independent enzymes containing several oxygen sensitive redox centers and transition metals, such as tungsten, molybdenum and iron [37]. It is also an important precursor for the production of biological fuels in the form of hydrogen, methane and potentially methanol [38].

I.4. The molybdenum and tungsten containing enzymes

Although molybdenum ($_{42}$Mo) and tungsten ($_{74}$W) are trace elements of the Earth's crust, they are almost ubiquitous in all living organisms [39–41]. These metals, when inserted in a cofactor on the active center of several enzymes, are responsible for catalyzing key reactions of the biogeochemical cycle of sulfur (sulfite oxidase, polysulfide reductase), nitrogen (nitrate reductase, nitrogenase) and carbon (formate dehydrogenase, carbon monoxide dehydrogenase) [39].

The incorporation of these metals in different cofactors, along with minor differences in the substrate-binding pocket, allows them to be fine-tuned to perform completely different functions in living cells. Exception made for the multinuclear heterometallic [$MoFe_7S_9$] cluster, found only in prokaryotic nitrogenases, all other known mononuclear molybdenum- and tungsten-containing enzymes (Mo/W-enzymes) possess a pyranopterin cofactor, commonly referred in the literature as molybdopterin, since it was believed it was present only in molybdenum enzymes. The cofactor structures that coordinate the metal in these enzymes are depicted in Figure I.6.

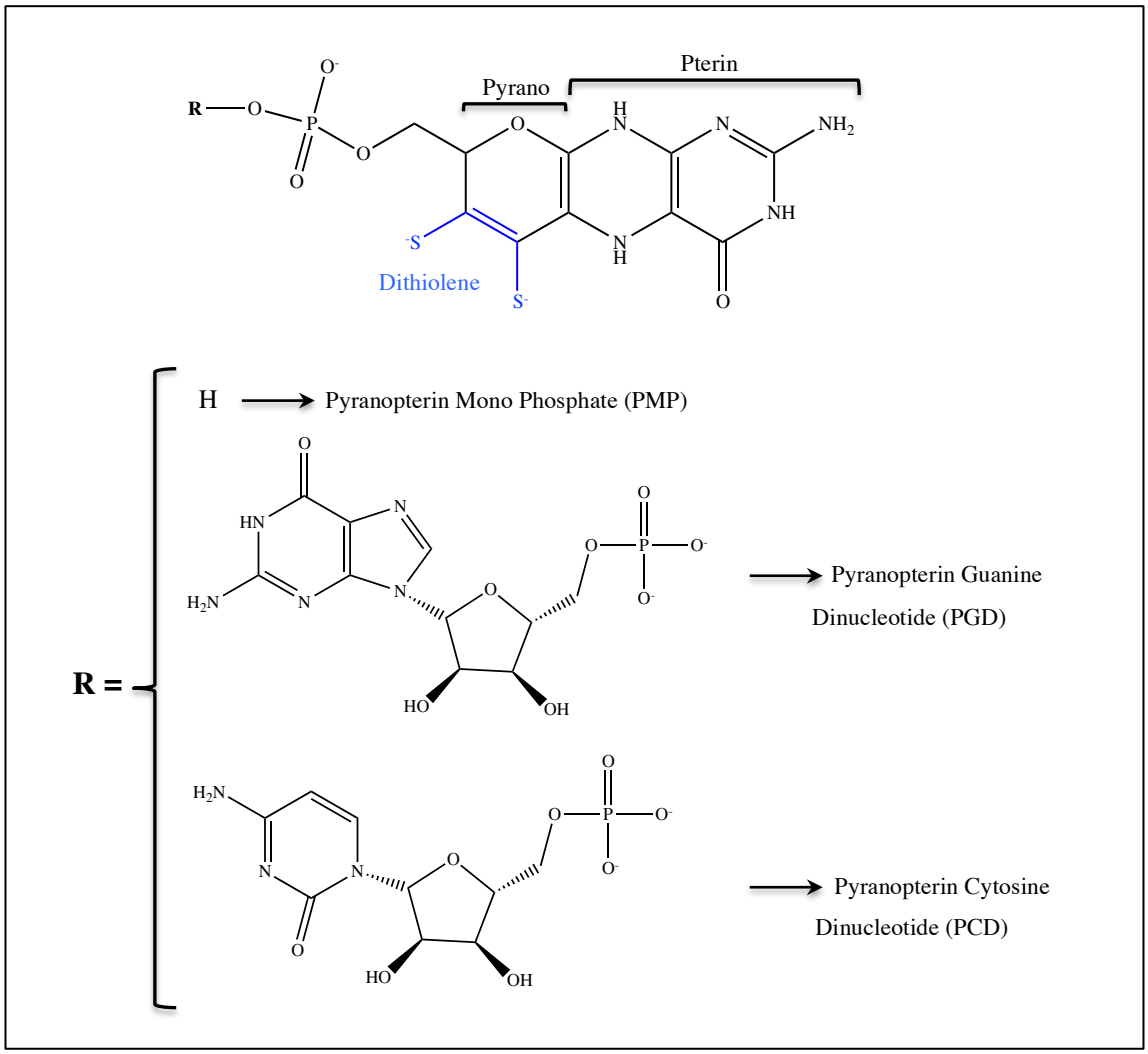

Figure I.6 – Pyranopterin cofactor present in mononuclear Mo/W-containing enzymes [39,40]**.** Top: Structure of the pyranopterin cofactor. Bottom: The cofactor can be found in the simplest monophosphate form (R is a hydrogen atom), or esterificated with different nucleotides (R can be one cytosine monophosphate or guanosine monophosphate).

These mononuclear enzymes can be sorted in four families, according mainly to their active site structure [39,40,42,43]:

The xanthine oxidase (XO) family harbors the molybdenum ion coordinated by one pyranopterin monophosphate (PMP) or pyranopterin cytosine dinucleotide (PCD) molecule. Oxygen, sulfur or selenium completes the coordination sphere of molybdenum in a distorted square pyramidal geometry, as shown in Figure I.7. A

common and distinguishable feature in the cofactor of members of this family is the inexistence of a covalent attachment to the polypeptide chain.

The sulfite oxidase (SO) family enzymes, as opposed to those of the XO family, have a sulfur atom from a cysteine residue coordinating directly to the molybdenum and a single pyranopterin cofactor that, together with the cysteine residue, anchors the molybdenum to the protein. An oxo and hydroxo groups, complete the coordination sphere of the molybdenum ion, as depicted in Figure I.7.

The tungsten aldehyde oxidoreductase family comprises enzymes with tungsten at their active sites. As Figure I.7 shows, the metal is coordinated by two pyranopterin guanine dinucleotide (PGD) or two PCD cofactors in a similar fashion to those of the dimethyl sulfoxide reductase family.

The dimethyl sulfoxide (DMSO) reductase family encloses Mo/W-enzymes belonging exclusively to prokaryotes that mainly catalyze oxygen atom transfer reactions, namely oxidation/reduction and hydroxylation reactions. It is the largest family and the one with the utmost variability, both structurally and catalytically, as illustrated by Figure I.7. Yet, it is also the one where more similarities are found between the overall polypeptide fold of its catalytic subunits. Due to this variability, which is not limited to the atoms that compose the coordination sphere, but also to the amino acid residues that encompass the active site, this family can be further subdivided into subfamilies I, II and III:

- Subfamily I includes enzymes whose active sites are coordinated by a cysteine or selenocysteine such as periplasmatic nitrate reductases and formate dehydrogenases.

- Subfamily II groups enzymes in which the coordination sphere of the metal is completed by one or two oxygen atoms from an aspartate residue. Membrane-bound respiratory nitrate reductase and ethylbenzene dehydrogenase are examples of enzymes belonging to this subfamily.

- Subfamily III accounts for enzymes in which a serine side chain occupies the fifth coordination position of the metal ion. Examples of enzymes belonging to this subfamily are the DMSO reductase from *Rhodobacter capsulatus* and the trymethylamine N-oxide reductase from *Shewanella massilia*.

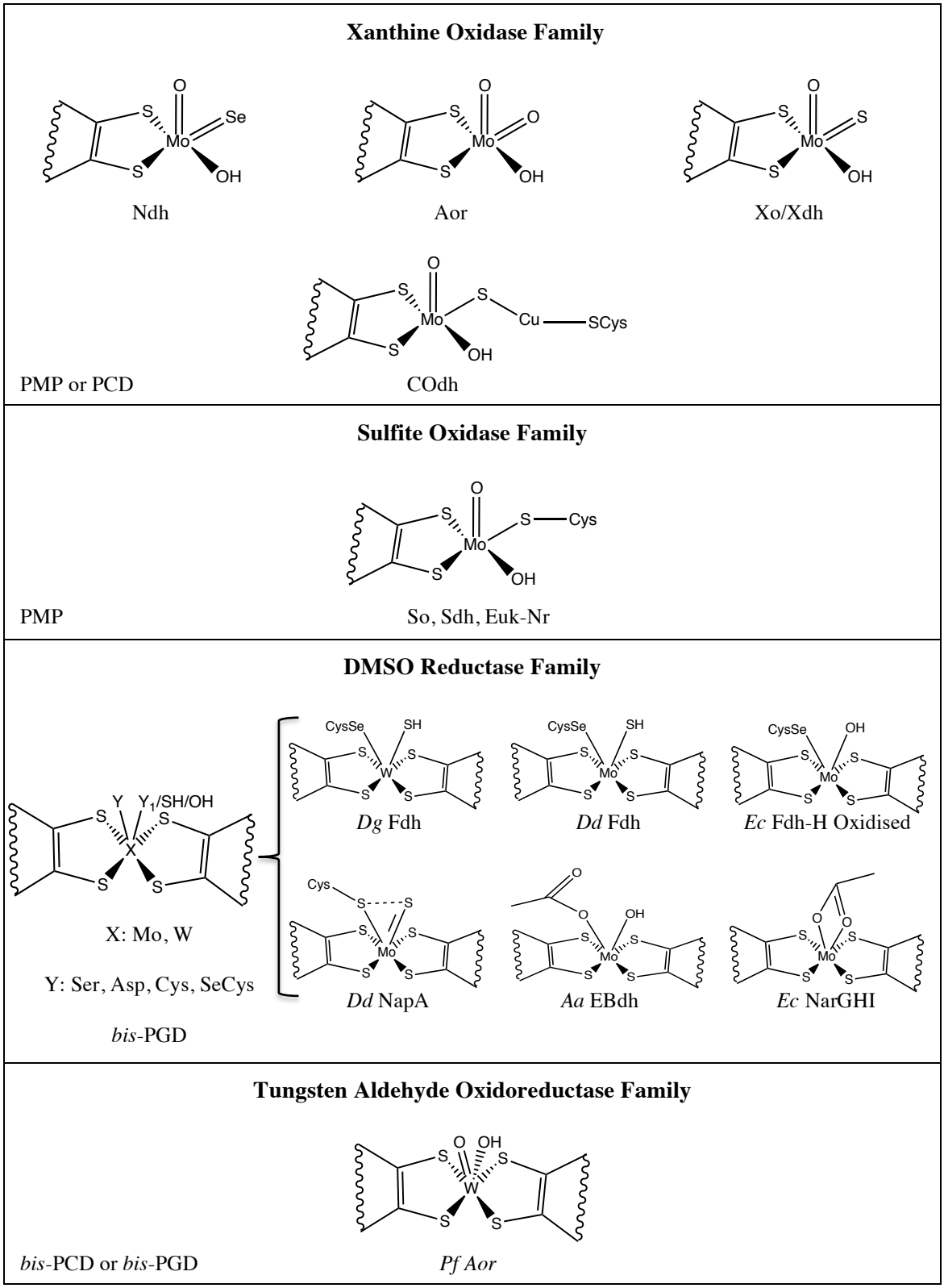

Figure I.7 – Active site structures amongst the different families of Mo and W pyranopterin-dependent enzymes [39,40]**;** (Xanthine Oxidase Family) Ndh: nicotinate dehydrogenase; Aor: aldehyde oxidoreductase; Xo/Xdh: xanthine oxidase/xanthine dehydrogenase; COdh: carbon monoxide dehydrogenase; (Sulfite Oxidase Family) So: sulfite oxidase; Sdh: sulfite dehydrogenase;

Euk-Nr: eukaryotic nitrate reductase; (DMSO Reductase Family): the metal at the active site (X) can be molybdenum or tungsten. The ligand Y can be a Serine (Ser), Aspartate (Asp), Cysteine (Cys) or a Selenocysteine (SeCys) residue and Y_1 can be a second ligand from the Y amino acid. *Dg* Fdh: *Desulfovibrio gigas* formate dehydrogenase; *Dd* Fdh: *Desulfovibrio desulfuricans* ATCC 27774 formate dehydrogenase; *Ec* Fdh-H: *Escherichia coli* formate dehydrogenase H; *Dd* NapA: *Desulfovibrio desulfuricans* ATCC 27774 periplasmatic nitrate reductase A; *Aa* EBdh: *Aromateleum aromaticum* ethylbenzene dehydrogenase; *Ec* NarGHI: *Escherichia coli* nitrate reductase GHI; *Pf* Aor: *Pyrococcus furiosus* aldehyde ferrodoxin:oxidoredutase. The pyranopterin cofactor coordinating the metal, in each family, is indicated on the bottom-left corner: PMP: pyranopterin monophosphate; PCD: pyranopterin cytosine monophosphate; PGD: pyranopterin guanosine monophosphate.

Figure I.8, depicts a schematic representation of the different coordination of the metal in the three subfamilies. Molybdenum or tungsten are hexa-coordinated, bound to four sulfur atoms from two dithiolene moieties from the two pyranopterins molecules and two other ligands, that account for their classification into one of the three subfamilies.

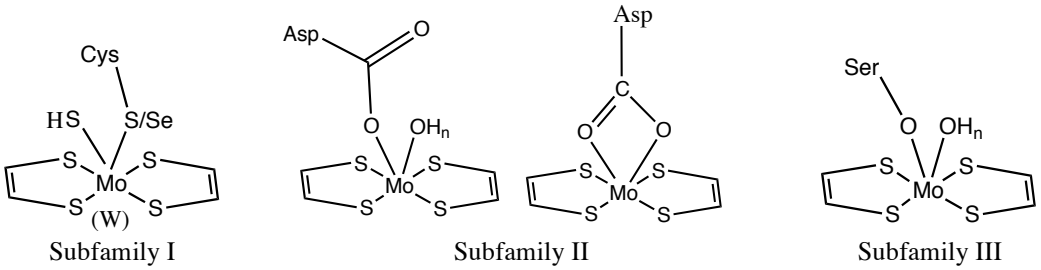

Figure I.8 – Different molybdenum coordination in the three subfamilies within the DMSOr family of Mo/W-enzymes.

Being the most diverse of the four families, both structurally and catalytically, there are members of the DMSOr family that, due to their singular characteristics, cannot be included into any of the three subfamilies. Examples of this diversity can be found in the arsenite oxidase from *Acaligenes faecalis*, which has no amino acid side chain coordinating the molybdenum atom, and the pyrogallol-phloroglucinol transhydroxylase from *Pelobacter acidigallici* that catalyzes non-redox reactions.

I.4.1. Formate dehydrogenase

Formate oxidation and CO_2 reduction are interconvertible processes that are catalyzed by a family of ubiquitous enzymes that can be found throughout all the domains of life [37,41,44,45].

The formate dehydrogenase family branches in two groups. The first group encompasses metal devoid NAD^+-dependent Fdhs. These enzymes are found mainly in aerobic organisms and catalyze, *in vivo*, the irreversible oxidation of formate to CO_2 coupled with the reduction of NAD^+ to NADH, according to Equation I.2 [25,46].

(eq. I.2)

$$HCOO^- + NAD^+ \rightarrow CO_2 + NADH$$

Apart from playing an important role in energy conversion reactions in plants, fungi and methylotrophic aerobic bacteria, metal devoid NAD^+-dependent Fdhs have been of central importance since the nineteen seventies, when they were used to solve a NADH regeneration problem that presented itself when redox enzymes were being used in the synthesis of organic chemicals [25]. Nowadays, these Fdhs are widely used for regenerating NADH in enzymatic-aided synthesis of optically active compounds. Degussa, a German company has developed an industrial scale process for the production of *ter*-L-leucine that relies on Fdh as a catalyst for NADH regeneration, in one of the largest enzymatic processes in pharmaceutical chemistry [47–49].

The second group of proteins includes all formate dehydrogenases that contain transition metals, such as molybdenum or tungsten associated with a PGD cofactor and iron in the form of iron-sulfur centers and/or hemes. Enzymes belonging to this group are mainly found in anaerobic prokaryotes, where they catalyze the two-electron oxidation of formate to CO_2 as follows [50]:

(eq I.3)

$$HCOO^- \rightarrow CO_2 + 2e^- + H^+ \qquad E^0 = -420 \text{ mV}$$

Among all enzymes that may catalyze CO_2 reduction, formate dehydrogenase is one of the most interesting to be used as a biocatalyst in biotechnological processes [25,34,51,52], and it is also one of the most promising catalysts for CO_2 scavenging and conversion into energy-bearing products [25]. Employing formate dehydrogenase as a biocatalyst for formate oxidation would result in safer fuel cell systems [52] whereas its application as a CO_2 reduction catalyst would turn formate into an alternative and safer biofuel [11,37,53–55]. When compared to hydrogen, formate is a non-flammable energy source, making its storage and transportation a more straightforward task. Additionally, the removal of CO_2 from the atmosphere by this process can be viewed as a bioremediation process, as it involves the conversion of an environmentally hazardous compound into a nonhazardous one [56]. The versatility of this enzyme is demonstrated by its employment in several research fields. Besides the research currently being performed, aiming at its use as a biocatalyst in bioremediation processes and biofuel production, it has also been key in the development of biosensors [57] and has found its way into organic chemistry were as a biocatalyst it allows for milder reaction conditions and improved selectivity [58].

The Fdh used in this work was isolated from *Desulfovibrio desulfuricans* ATCC 27774 (*Dd*), a sulfate reducing bacteria (SRB), belonging to the DMSOr family of Mo/W-enzymes. So, throughout this dissertation, NAD^+-independent Fdh enzymes will be abbreviated to Fdh.

I.4.1.1. Formate dehydrogenase – Structural Studies

Three Fdh crystallographic structures have been determined. Fdh-H isolated from *Escherichia coli* (*E. coli*), a Mo-containing enzyme (Mo-enzyme), was the first to be structurally characterized. It was found to be a monomeric enzyme with approximately 80 kDa, containing one [4Fe-4S] cluster and one molybdenum atom in a distorted trigonal prismatic geometry coordinated to four dithiolene sulfur atoms, from the two PGDs, a selenium atom, from a conserved SeCys residue, and a sulfur ligand [39,59]. However, in earlier crystallographic studies a loop close to the molybdenum active site was mistraced. This led to an erroneous interpretation of the electron density maps that placed the SeCys residue away from molybdenum. This mistake led the authors to

conclude this residue was not a molybdenum ligand, with implications to the reaction mechanism proposed [60].

Figure I.9 depicts the three-dimensional structure of the enzyme and the arrangement of the redox centers.

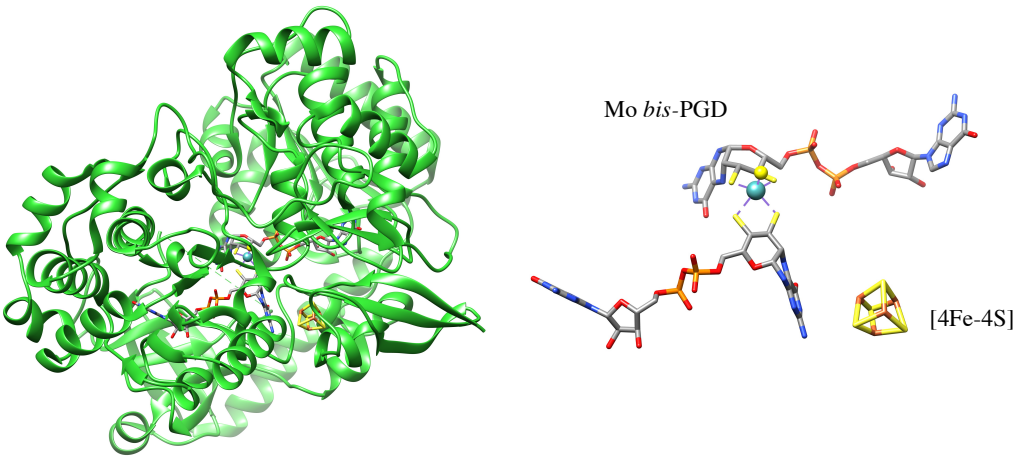

Figure I.9 – Fdh-H from *E. coli*. Left: Three-dimensional view of Fdh-H. Right: Arrangement of the redox centers shown in the same orientation. The structures shown are based on PDB file 2IV2 and were produced with Chimera v1.9rc.

Figure I.10 represents the active site of *E.* coli formate dehydrogenase, after being reduced by formate, and the conserved residues $SeCys_{140}$ (unbound), His_{141} and Arg_{333}.

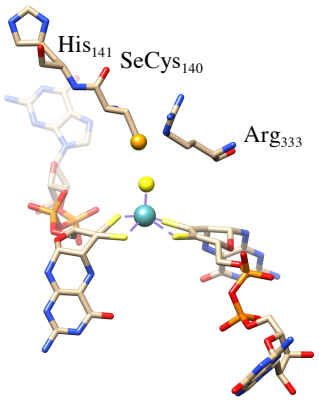

Figure I.10 - The Mo active site of *E. coli* Fdh-H, and conserved residues $SeCys_{140}$, His_{141} and Arg_{333}. The structure showed is based on PDB file 2IV2 and was produced with Chimera v1.9rc.

The second structure solved, depicted in Figure I.11, belongs to the membrane-bound Fdh-N, also a Mo-enzyme isolated from *E. coli*. It is a 510 kDa

$(\alpha\beta\gamma)_3$ heterotrimer whose subunits have 113, 32 and 21 kDa, respectively. In this enzyme the α subunit has two roles; as it harbors the Mo center and the *bis*-PGD cofactor it is the catalytic subunit. And, as it also harbors a [4Fe-4S] cluster it is also part of the electron transfer pathway. This pathway also encompasses four [4Fe-4S] clusters found in the β subunit and is completed by two heme *b* groups in the integral membrane γ subunit. Although the catalytic α domain of Fdh-N is substantially larger when compared to that of Fdh-H, its three-dimensional Mo domain is quite similar [61]. It is also composed of a molybdenum atom that adopts a distorted trigonal prismatic geometry and is coordinated by four dithiolene sulfur atoms, from the two PGD cofactors, a selenium atom, from a conserved SeCys residue, and a sulfur ligand.

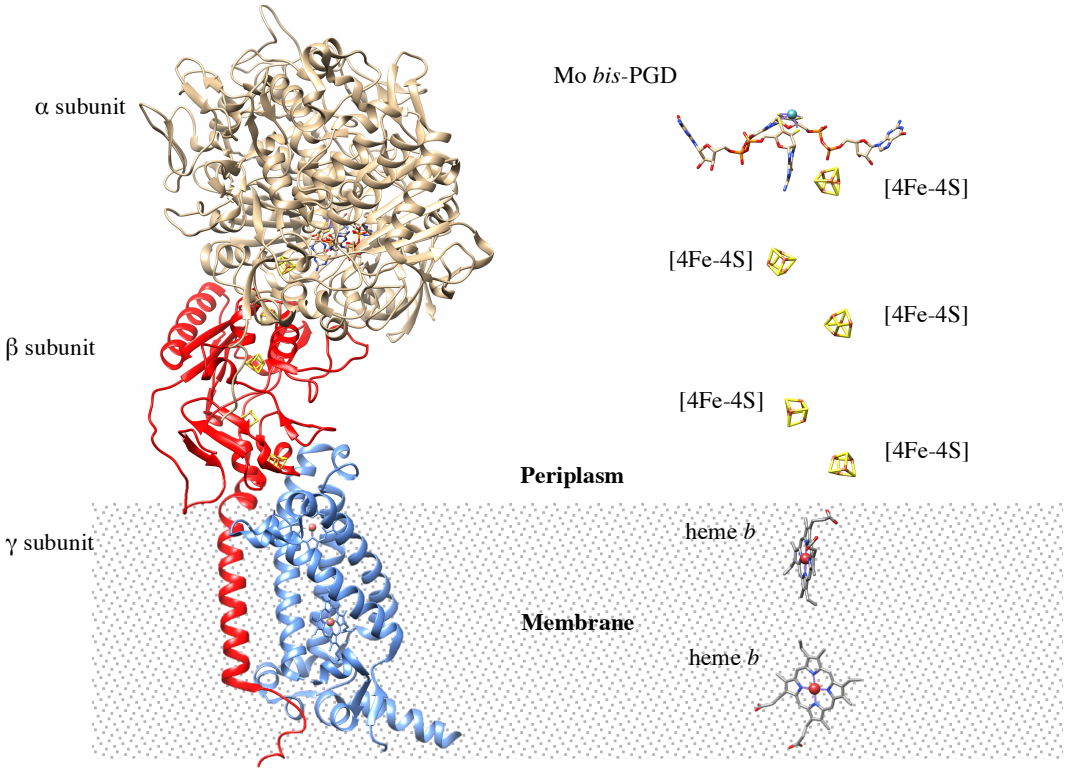

Figure I.11 – Fdh-N structure from *E. Coli*. Left: Three-dimensional view of Fdh-N. Right: Arrangement of the redox centers that compose the electron transfer pathway. The structures shown are based on PDB file 1KQF and were produced with Chimera v1.9rc.

In the active site of Fdh-N, as in the active site of Fdh-H, there are three conserved amino acid residues, $SeCys_{196}$, His_{197} and Arg_{446}. The active site of Fdh-N and the conserved amino acid residues are represented in Figure I.12.

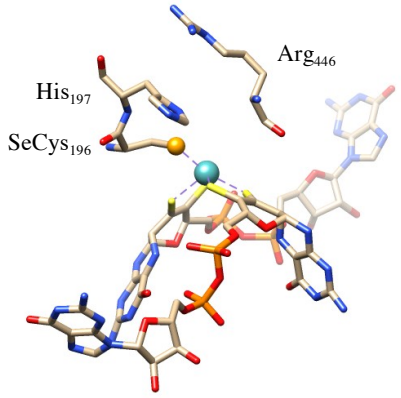

Figure I.12 – The molybdenum-containing active site of Fdh-H, isolated from *E. coli*, and the conserved residues $SeCys_{196}$, His_{197} and Arg_{446}. The structure presented is based on PDB file 1KFQ and was produced with Chimera v1.9rc.

The third Fdh structure solved belongs to the Fdh of the SRB *Desulfovibrio gigas* (*Dg*). This enzyme is a αβ heterodimer whose subunits have 92 and 29 kDa. Its larger α subunit harbors the W active site. In it, the tungsten is coordinated by two PGDs, a SeCys and one sulfur ligand, adopting a distorted trigonal prismatic geometry. The α subunit of this enzyme encompasses the catalytic center, where the molybdenum atom is located, and is also the starting point for the electron transfer pathway via its [4Fe-4S] cluster. This pathway is completed by three additional [4Fe-4S] clusters in the β subunit (Figure I.13) [62–64].

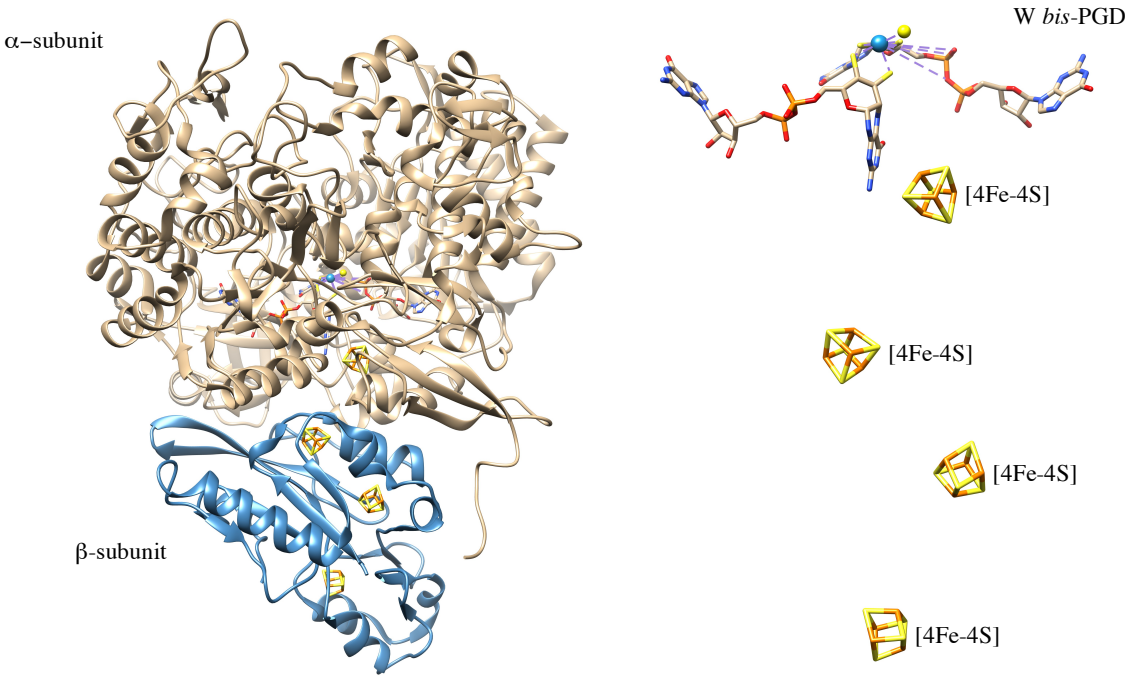

Figure I.13 – Fdh structure from *D. gigas*. Left: Three-dimensional view of W-Fdh from *D. gigas*. Right: Arrangement of the redox centers that compose the electron transfer pathway in the same orientation. The structures shown are based on PDB file 1H0H and were produced with Chimera v1.9rc.

Figure I.14 depicts the W active site of *D. gigas* Fdh and the conserved amino acid residues, $SeCys_{158}$, His_{159} and Arg_{407}.

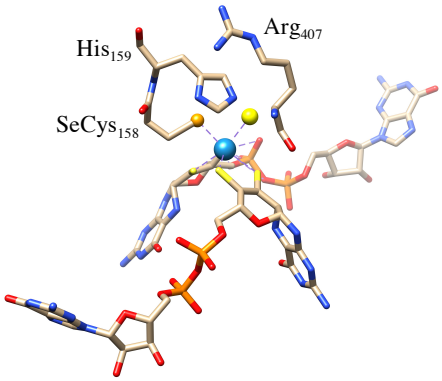

Figure I.14 – The W active site of *D. gigas* Fdh and the conserved residues $SeCys_{158}$, His_{159} and Arg_{407}. The structure presented is based on PDB file 1H0H and was produced with Chimera v1.9rc.

Although, no crystallographic structure for the *D. desulfuricans* Fdh, has been determined, it has already been extensively characterized in previous studies. It is reported to be a αβγ heterotrimer of 88, 29 and 16 kDa, respectively. The α subunit

includes the molybdenum site and one [4Fe-4S] cluster, the β subunit holds one [4Fe-4S] cluster and finally the γ subunit harbors four *c*-type hemes [44,50,65].

As the structures of the three Fdhs were found to exhibit a high similitude between their α subunits, it is reasonable to assume that the α subunit of the Fdh from *D. desulfuricans* should also present the same overall fold [40,61,66]. As it is reasonable to assume that other structural motifs might also be present. Such motifs may include the formate cleft, a positively charged lined funnel-shaped channel used by formate to reach the active site, a putative proton channel (identified in Fdh-H and in the W-Fdh from *Desulfovibrio gigas),* oriented perpendicular to the formate cleft, coated with protonatable glutamic and aspartic acid side chains, and a hydrophobic channel, that may be responsible for the release of CO_2 [62].

Figure I.15, depicts an alignment of the three structures referred earlier and of the conserved amino acids residues at the active site a SeCys, a neighboring His and an Arg that is thought to stabilize the negatively charged substrate in the active site [39,62,66]. The root-mean-square deviation (RMSD) of the amino acid chain for this alignment is 1.1 Å, demonstrating their overall similarity.

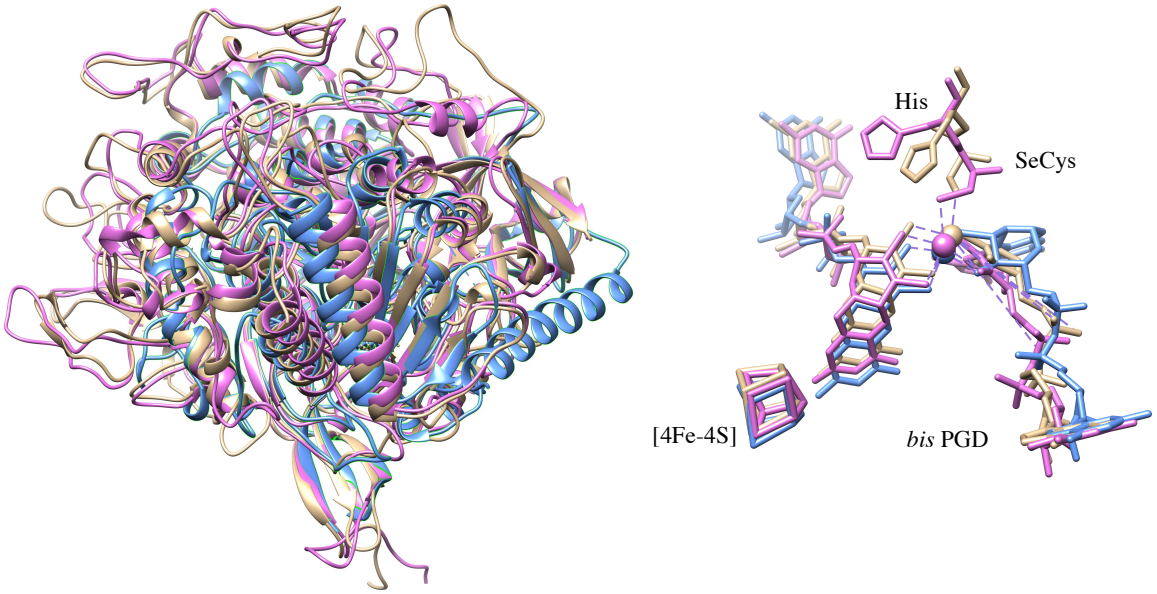

Figure I.15 – Alignment of the α subunits of Fdh-H (purple) and Fdh-N (beige) from *E. coli* with the α subunit of Fdh from *D. gigas (blue*) exhibiting an RMSD of 1.1 Å. Left: Overall superimposition of the three α subunits. Right: Detail of the active centers and of the conserved residues.

I.4.1.2. Formate dehydrogenase – Mechanistic Studies

NAD^+-independent formate dehydrogenases catalyze the oxidation of formate to carbon dioxide, according to the reaction depicted below.

(eq. I.4)

$$HCOO^- \rightarrow CO_2 + 2e^- + H^+$$

As was showed in Figure 1.7, the metal in the active center of *Desulfovibrio desulfuricans* Fdh is hexa-coordinated in a distorted trigonal prismatic geometry. Thus, no free coordination position exists for the substrate to bind and interact with the molybdenum ion. Three reaction mechanisms for formate oxidation by Fdh were proposed, by Boyington *et al*. (1997) [59], Raaijmakers *et al*. (2006) [60] and Mota *et al*. (2011) [66]. The differences between the three proposals are the occurrence, or not, of a direct coordination of the SeCys residue to the Mo ion throughout the catalytic cycle and the role of the conserved amino acids in the substrate-binding pocket. The first reaction mechanism, proposed by Boyington *et al*., was based on crystallographic data obtained for Fdh-H isolated from *E. coli*. This reaction mechanism proposes that catalysis is initiated with the coordination of the oxygen from formate to the oxidized Mo ion, displacing the –OH ligand while formate is being stabilized by the conserved residues His_{141} and Arg_{333} (Figure I.16, A➔B). The Se atom captures the α-proton of formate, two electrons are transferred to the Mo ion and CO_2 is released (Figure I.16, B➔C). Active site regeneration starts with an electron transfer from the Mo ion to the [4Fe-4S] cluster through the PGD moiety (Figure I.16, C➔D) and is completed with the oxidation of the Mo ion from Mo(V) to Mo(VI). This oxidation is achieved with a proton transfer from the $SeCys_{140}$ residue to the His_{141} residue followed by a second electron transfer from the Mo ion to the electron pathway (Figure I.16, D➔A).

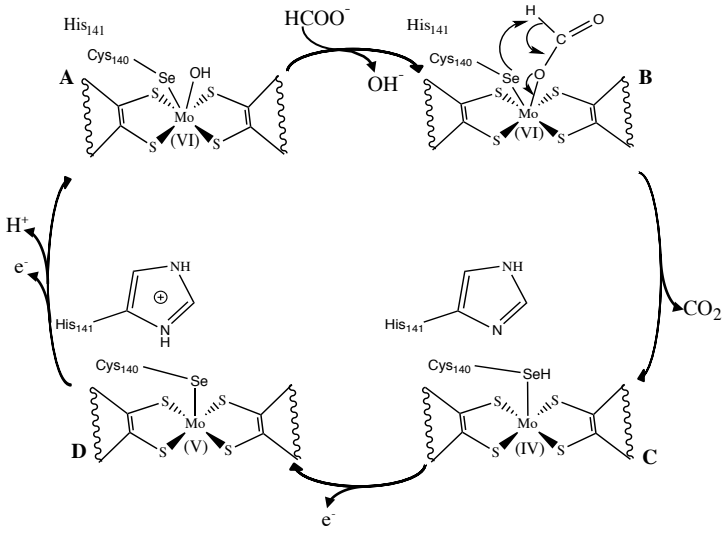

Figure I.16 – Reaction mechanism of formate oxidation by Fdh, proposed by Boyington *et al*. [59].

The second reaction mechanism proposed was based in the revised crystallographic structure of the formate-reduced Fdh-H from *E. coli*. In the original mechanism, proposed by Boyington *et al*., the SeCys residue was bound to molybdenum after reduction of the enzyme by formate. Raaijmakers *et al*. re-evaluated the crystallographic data and found that a loop close to the molybdenum active site was mistraced leading to the wrongful placement of catalytic relevant residues such as $SeCys_{140}$. After data re-evaluation it was found that this residue was no longer bound to the metal after the reduction of the enzyme with formate. As this interpretation was incompatible with the originally proposed reaction mechanism a new mechanism was proposed (Figure I.17). Before being reduced by formate, the SeCys residue is coordinated to the Mo ion (Figure I.17, A). Formate approximation, frees a coordination position for its binding to the active site, as it triggers the release of SeCys and the stabilization of its selenol group by the Arg residue. Then, the selenol group from the SeCys abstracts the α-proton of formate which is readily transferred to the His residue. CO_2 is released while two electrons are transferred to the Mo ion (Figure I.17, B➔C). Active site regeneration is achieved through binding of the selenol group to the Mo ion and its oxidation with electron transfer to the [4Fe-4S] cluster (Figure I.17, C➔A).

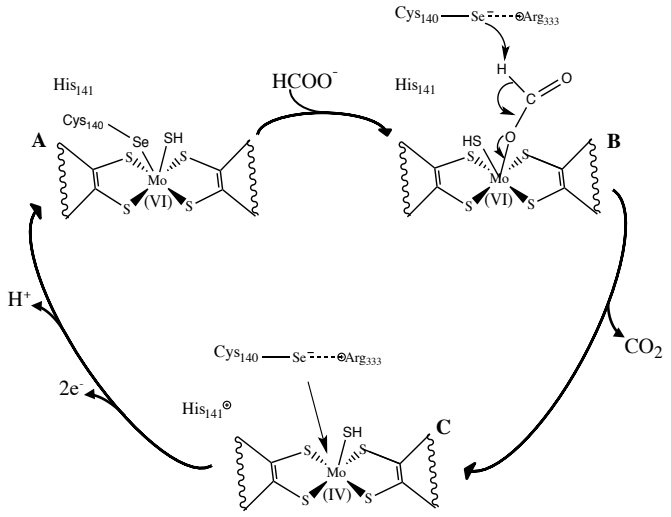

Figure I.17 - Reaction mechanism for formate oxidation by Fdh, proposed by Raaijmakers *et al.* [60].

Leopoldini *et al*. [67] assessed the energy barriers involved in each of these two proposed mechanisms and concluded that the second proposal is kinetic and thermodynamically more favorable, and that the reaction of proton abstraction from formate to the Se atom is more efficient when the SeCys residue is not a ligand at the Mo site.

The latest reaction mechanism to explain the two electron oxidation of formate to CO_2 was proposed by Mota *et al*. (2011) [66]. This mechanism requires the rearrangement of the sulfur atom coordinated to the metal, through a process known as the sulfur-shift, depicted in the top of Figure I.18.

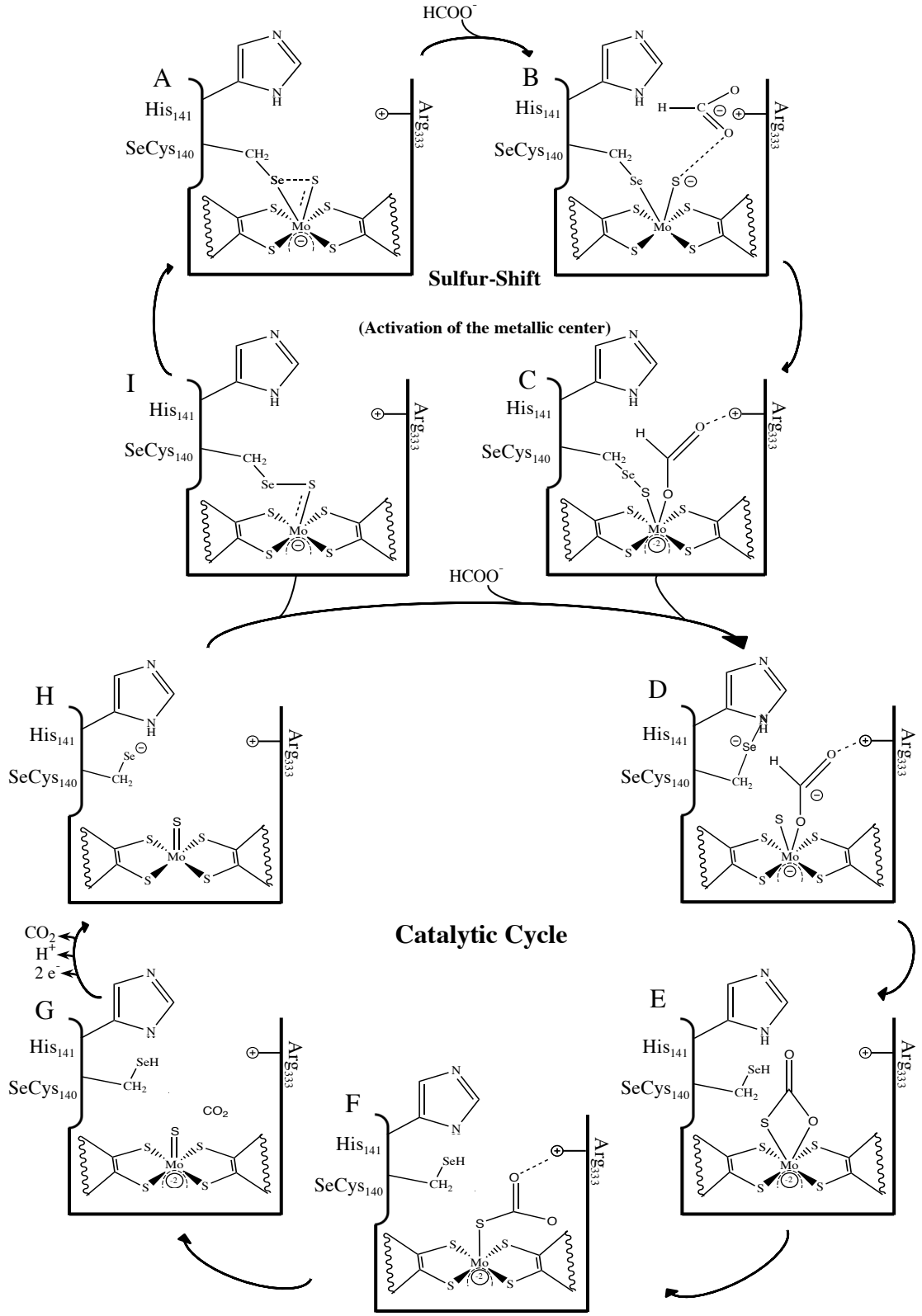

Figure I.18 – Reaction mechanism proposed for Fdh activation and formate oxidation as proposed by Mota, *et al*. (2011). Adapted from [66]. Top: Activation of the metallic center of Fdh via sulfur-shift. Bottom: Catalytic cycle for formate oxidation by Fdh.

In its oxidized, and inactive, form the active center of Fdh has a molybdenum ion in a Mo(VI) oxidation state. In this state, the sulfido (S_i) and SeCys ligands form a quasi-covalent bond with the molybdenum ion (Figure I.18, scheme A). As the formate anion reaches the substrate-binding pocket its negative charge is buffered by the conserved Arg residue and by the two pyranopterins (Figure I.18, scheme B). Further approach from formate to the Mo (VI) ion triggers the insertion of the S_i between the bond of the selenium atom and the molybdenum ion with the simultaneous bond of formate to the molybdenum ion. (Figure I.18, scheme C). Throughout these activation steps the metal remains hexa-coordinated and at the final step the sixth ligand is formate and Fdh becomes active. Formate oxidation involves several steps. The first being the cleavage of the bond between the selenol group from the SeCys and the S_i followed by simultaneous establishment of a hydrogen bond between the selenol group and the conserved His residue (Figure I.18, scheme D). Next, the selenol group from the SeCys abstracts the proton of formate, leading to the cleavage of the hydrogen bond to the conserved His while simultaneously forming a new bond between S_i and the carbon from carbon dioxide (Figure I.18, scheme E). The first step for the release of carbon dioxide involves breaking the Mo–O bond, while maintaining the carbon dioxide molecule connected to the active site through a S_i–C bond. (Figure I.18, scheme F). The release of the carbon dioxide molecule is accomplished through the cleavage of the S_i–C bond and the formation of a double bond between the S_i and Mo (Figure I.18, scheme G). The next step, involves the transfer of the proton attached to the SeCys residue and active site oxidation from Mo(IV) to Mo(VI) (Figure I.18, scheme H). Following this step, active site regeneration may follow two paths. If another formate molecule is present the S_i–Mo bond is displaced and formate will bind to the penta-coordinated molybdenum (Figure I.18, scheme D). However, if no formate molecule is available the SeCys residue binds to the S_i (Figure I.18, scheme I) and the SeCys–Mo bond is re-established (Figure I.18, scheme A).

I.5. Subject and objective of this work

The need for CO_2 valorization instead of its storage is necessary to help us overcome the energy crisis derived from both, the near end of fossil fuels and the increasing energy demand in emergent nations. To accomplish this goal, more research will have to focus on CO_2 sequestering and in finding carbon-neutral or carbon-negative strategies to handle with declining fossil fuel supplies and with the environmental impact caused by their usage.

The use of formate dehydrogenase in the conversion of CO_2 into a biofuel could lead to significant changes in the economic paramount, while at the same time significantly reduce GHG emissions. Although the use of enzymes at an industrial scale poses a serious difficulty due to the fragile nature of these systems when compared with synthetic catalysts, there is an increasing demand for catalytically perfect systems, with high turnover constants and low running costs. And one expects this will act as a driving force, attracting investment for this field of study and eventually lead to significant improvements in the development of robust synthetic catalysts.

The conversion of CO_2 to formate has been reported and studied in a limited number of NAD^+-independent formate dehydrogenases and it was thought to be exclusive of W-containing Fdhs. The explanation for this was linked to tungstoenzymes ability to catalyze low potential reduction reactions leading to the assumption that reduction of CO_2 to formate is W-dependent [11,61,68,69].

The main purpose of this work was to demonstrate that NAD^+-independent molybdoenzymes could also catalyze the reduction of CO_2 to formate. To accomplish this, a Mo-Fdh will be isolated from the SRB *Desulfovibrio desulfuricans* ATCC 27774. As a large amount of pure enzyme will be needed it will be necessary to determine which type of culture media allows for a greater development of the bacterial cells. Afterwards, the media will be narrowed to the one that allows a superior Fdh expression and the harvest conditions will be optimized to permit a higher Fdh recovery from the growth extracts. Following growth optimization solution, kinetic assays will be performed to determine the kinetic parameters K_M and k_{cat} for the oxidation of formate to carbon dioxide. Lastly, we will aim to determine if this Mo-enzyme is able to

catalyze the inverse reaction, carbon dioxide reduction to formate, allowing for its use as a biocatalyst in an energetically efficient CO_2 fixation process that might be directed towards bioremediation or as an alternative and renewable energy source.

II. MATERIALS AND METHODS

II. MATERIALS AND METHODS

All reagents used throughout this work were of analytical grade. Table VI-18, in appendix, summarizes the brand and the purity of the reagents used.

II.1. Bacterial strain, culture media and growth conditions

D. desulfuricans ATCC 27774 (*Dd*) cells were used in all the experiments. These were grown in several media at 37ºC under strict anaerobic conditions. To establish anaerobiosis, the flasks containing the medium were flushed with argon (Praxair Pure Argon-3X) before being autoclaved, making its gas phase 100% argon.

Since the bacterial strain was maintained in VMN medium, firstly the cells needed to be adapted to the different test media. For this medium change, *Dd* cells were inoculated in flasks where 10% of the VMN medium volume was replaced by the same volume of one of the other media where the cells were to be grown. After a 24-hour incubation period these cells were inoculated into flasks where an equal volume of the test medium replaced 20% of the VMN medium. Again, after a 24-hour incubation at 37ºC the cells were transferred to another flask and the procedure was repeated for 30%, 50%, 75%, 90% and total replacement of the VMN medium for each of the test media according to the scheme presented below.

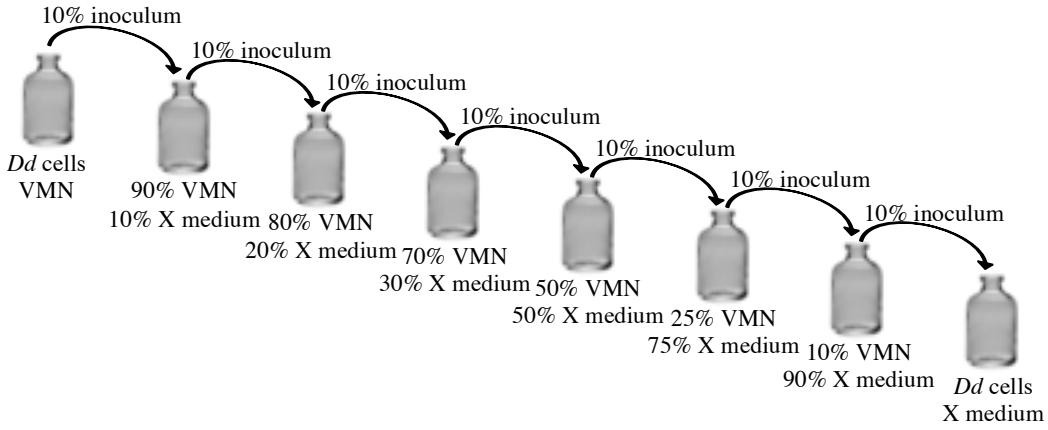

Figure II.1 – Schematic representation of the acclimatization procedure of *D. desulfuricans* cells to the different media tested. Each arrow represents an inoculation that is 10% of the total growth volume. X media represents each of the media tested, ATCC 42, ATCC 1249, ATCC 2755, ATCC 27774 and LYSC. Between each involution the cells were allowed a 24-hour incubation period at 37ºC.

After adapting the cells to each of the test media, a first screening was done to determine which of the test media, ATCC 42, ATCC 1249, ATCC 2755, ATCC 27774, LYSC and VMN allowed for a higher cell mass to be harvested. Employing an inoculum representing 10% of the total growth volume, growth in each media was evaluated by visual inspection, after a 24-hour incubation period at 37ºC. If there was little propagation the cells were allowed another 24-hour incubation period at 37ºC as schematized below.

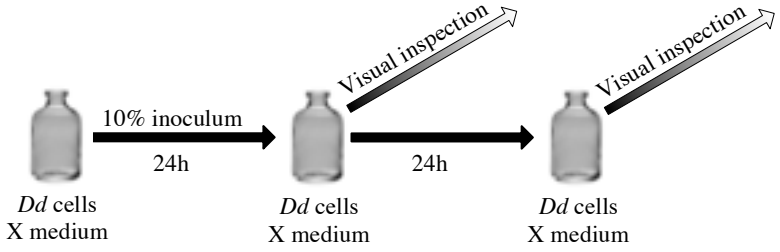

Figure II.2 – Schematic representation of the screening done to determine which of the test media would allow for a higher cell mass to be harvested. X media represents each of the media tested, ATCC 42, ATCC 1249, ATCC 2755, ATCC 27774, LYSC and VMN.

If after a 48-hour incubation period there was still little propagation the medium was discarded.

After this assessment, a second screening, intended to determine which of abovementioned media allowed for a higher expression of Fdh was done. The composition of the media employed in the last phase of these screenings (VMN, ATCC medium 1249, ATCC medium 2755 and M medium), is summarized in Table II-1. For detailed preparation procedures and composition of some of the media components please refer to appendix VI.1.

Table II-1 – Culture media compositions, per liter.

	VMN*	ATCC 1249*	ATCC 2755**	M*
KH_2PO_4	0.5 g	-	-	-
$K_2HPO_4.3H_2O$	-	0.66 g	0.66 g	0.47 g
$MgSO_4.7H_2O$	-	4.1 g	2.0 g	-
$NaNO_3$	2.4 g	-	-	2.28 g
Na_2SO_4	-	-	1.0 g	-
NH_4Cl	1.0 g	1.0 g	1.0 g	1.9 g
$MgCl_2.6H_2O$	0.05 g	-	-	1.55 g
$CaCl_2.2H_2O$	0.04 g	-	0.1 g	0.2 g
$CaSO_4.2H_2O$	-	1.3 g	-	-
Na-Lactate	6.0 g	3.5 g	2.0 g	10 mL
Na-Citrate	0.3 g	5.7 g	-	-
$FeCl_2.4H_2O$	0.003 g	-	-	0,67 g
$Fe(NH_4)_2(SO_4)_2$	-	2% (v/v)◆	-	-
$FeSO_4.7H_2O$	-	-	0.5 g	-
Wolfes Elixir	1 mL	-	-	-
NZCYM Broth	2.0 g	-	-	-
Triptone	2.0 g	-	-	-
Vitamin Solution	2 mL	-	-	-
Yeast Extract	-	1.0 g	1.0 g	0.95 g
Na-thioglycolate	-	-	0.1 g	-
Ascorbic Acid	-	-	0.1 g	-
$Na_2S.3H_2O$	-	-	-	10 mL❖
"Fauque" Oligoelements	-	-	-	10 mL

* – pH adjusted to 6.5 ± 0.05; ** – pH adjusted to 6.8 ± 0.05; ❖ – 1% (w/v) $Na_2S.3H_2O$ solution;

◆ – 5% (w/v) $Fe(NH_4)_2(SO_4)_2$ solution;

The bacterial cells were cultivated at 37ºC, in anaerobic flasks with volumes ranging from 10 to 100 mL of medium with inoculums ranging from 2 to 10% of the total flask volume and cell harvest was done at mid exponential or stationary phases. In either case, growth was accompanied by optical density (O. D.) value measurements at 600 nm using a Shimadzu UV 160A spectrophotometer.

Growths under hydrogen were done inside a sealed anaerobic bag at 37ºC, in 100 mL anaerobic flasks under a continuous flow of 100% H_2.

Cultures were periodically checked for possible contamination employing optical microscopy. Figure II.3, depicts a pure culture judging from the similar morphology of the cells.

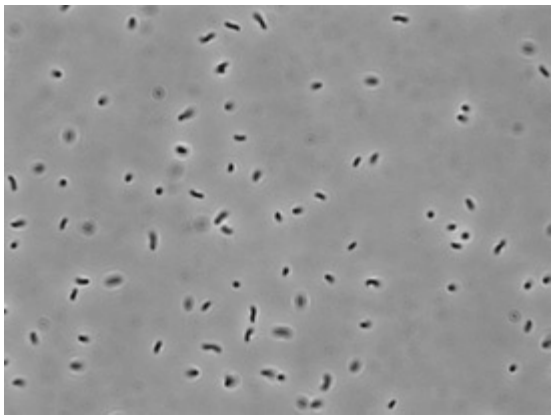

Figure II.3 – *D. desulfuricans* cells, magnified 1000x.

To obtain enough Fdh to perform the kinetic assays, a 200 L reactor growth was outsourced. This growth was done with an inoculum that was 2% of the total growth volume, and cells were harvested at the end of the exponential phase.

II.2. Soluble extract preparation

Cells from each condition described above were collected at two different stages of growth, one set was collected at the end of the exponential growth phase and another set was collected at mid-exponential growth phase. Cell harvest was accomplished by centrifugation of the culture medium at 7000 *g* for 15 min at 4ºC in a Sigma 3K30

centrifuge. After centrifugation the pellet was resuspended in 10 mM Tris-HCl buffer (pH 7.6) to a cell density of 0.1 g cells (wet weight) per mL.

Periplasmatic soluble extracts were prepared by subjecting this cell suspension to 4 freeze-thaw cycles followed by centrifugation at 7000 *g* for 40 minutes to remove spheroplasts. The resulting periplasmatic supernatant was later used for activity measurements.

To obtain the cell soluble extract the cells were resuspended in 10 mM phosphate buffer (pH 7.6), to a cell density of 3 g cells (wet weight) per mL. These cells were then subjected to a pressure of 20000 psi in a French Pressure Cell Press (Thermo Electron Corporation) and this sample, total cell soluble extract, was also used for activity measurements. In some samples, 1 mM phenylmethylsulfonyl fluoride (PMSF) and 1 mM dithiothreitol (DTT) were also added to the ressuspension buffer before disrupting the cells in the French Press. Such samples are clearly identified in the results section. A flowchart of these procedures is depicted in Appendixes VI.3 and VI.4.

II.3. In gel activity assays

In Appendix VI.2, a detailed description of the solutions employed for the preparation of the polyacrylamide gels used throughout this work is given.

In gel activity assays were performed by placing equal amounts of the total protein content, derived either from the periplasmatic soluble extract or from total soluble extract, onto 7.5% polyacrylamide gels. Electrophoresis was performed at a constant current of 40 mA *per* gel. The activity assay was done at room temperature by placing the gels in rubber stoppered falcon tubes containing: 10 mM HCOONa, 130 mM β-mercaptoethanol and 60 mM Tris-HCl buffer (pH 8.0). The gels were incubated for 15 minutes in anaerobic conditions, assured by the bubbling of argon in the activity buffer. Afterwards, methyl viologen (MV) was added, to a final concentration of 7.5 mM, and the solution was further incubated in order for the blue activity bands to develop. After this step the activity bands were fixed with 2,3,5-thiphenyltetrazolium chloride (final concentration of 7.5 mM). In all assays a (positive) control consisting of pure Fdh was loaded into the gel.

II.4. Fdh purification

Dd Fdh was isolated as described in [65] with some minor modifications as reported in [50]. The cells were cultured in VMN medium and collected by centrifugation at the end of the exponential phase. Then the cells (170 g wet weight, from a outsourced 200 L reactor) were resuspended in 10 mM Tris-HCl buffer and ruptured in a high-pressure homogenizer at 9000 psi. After centrifugation (10000 *g*; 45 minutes; Sigma 3K30 centrifuge) and ultracentrifugation (180000 *g*; 60 minutes; Beckman L-70 ultracentrifuge) the supernatant was dialyzed overnight against 10 mM Tris-HCl buffer and loaded onto an anionic exchange column (DEAE Bio Gel, equilibrated with 10 mM Tris-HCl). Elution was achieved with a linear gradient (10 to 300 mM Tris-HCl) in 3 column volumes. Fdh activity was determined in each collected fraction following the procedure described in Section II.3 placing equal volumes of each of the fractions on 7.5% polyacrylamide gels.

At this point, no other purification procedures were done. Further purification steps are presented in a flowchart that is depicted in appendix VI.5.

II.5. Protein content quantification

Protein quantification was done employing the Lowry method, with bovine serum albumin as standard. This procedure is described in detail in [70].

II.6. Preliminary Fdh reduction studies

Fdh reduction assays were accomplished by monitoring the spectrum of the protein between 380 and 600 nm with a Shimatzu UV-2500PC Series spectrophotometer. The assays were performed in a 1 cm optical path length quartz cell with magnetic stirring and stoppered with rubber caps. The 650 µL reaction mixture was composed of 60 mM Tris-HCl buffer (pH 8.0) and 0.8 µM Fdh; sequential additions of 50 µM DTT, 83 and 147 µM sodium formate and sodium dithionite were done when the previously acquired spectrum was stable.

All solutions were deaerated with purified argon for 30 minutes and all additions were made with gas tight syringes.

II.7. Steady-state kinetic assays

Steady-state kinetic assays were performed under an argon atmosphere at room temperature by monitoring the reduction or oxidation of either methyl viologen or benzyl viologen at 607 and 555 nm, respectively, using a Shimatzu UV-2500PC Series spectrophotometer. The assays were done employing the same experimental setup as in the preliminary Fdh reduction studies, in Section II.6.

For the formate oxidation reaction, the 2 mL reaction mixture was composed of 60 mM Tris-HCl buffer (pH 8.0), sodium formate concentrations ranging from 0 to 5 mM, 7.5 mM benzyl or methyl viologen, 133 mM β-mercaptoethanol or DTT, in concentrations from 0 to 2 mM concentration. Enzyme concentrations ranged between 0 and 50 nM. The reaction mixture composed by enzyme, buffer and β-mercaptoethanol or DTT was firstly incubated for 7 minutes. Then formate was added and incubated for another 30 minutes. Lastly, to begin the reaction benzyl or methyl viologen were added.

In the carbon dioxide reduction reaction, the 2 mL reaction mixture was composed of 100 mM phosphate buffer (pH 6.8), CO_2 concentrations varying from 0 to 95 μM, 312.5 μM benzyl or methyl viologen, and enzyme in concentrations varying between 0 and 15 nM.

All reagents were deaerated with purified argon prior to the start of the assays and all additions were made with gas-tight syringes.

Sodium dithionite or zinc were used to reduce the viologens, either benzyl or methyl, in the reaction mixture. In the assays where the zinc pellets were used the viologen was already reduced when it was added to the reaction mixture. In these assays, the reduced mediator was prepared beforehand incubating a zinc tablet with the viologen for a period of time ranging from 5 to 24 hours.

After baseline stabilization CO_2 was added in the form of carbonate. The reaction rates were measured as the difference between the slopes of the chemical re-oxidation of the viologens (baseline) and the initial slope after CO_2 addition.

Deionized water was used in all kinetic assays. For carbon dioxide reduction assays the buffer and sodium carbonate solutions were decarbonated, prior to their utilization, by boiling the water employed in their preparation for 15 minutes and then purging it with argon.

Formate/carbon dioxide concentrations were calculated employing the molar extinction coefficient for reduced benzyl viologen (BV) (ε_{555} = 12 mM^{-1} cm^{-1}) [65]. Under these experimental conditions, one enzymatic unit (U) corresponds to 1 μmol of formate oxidized/carbon dioxide reduced (2 μmol of BV reduced/oxidized) *per* minute.

II.7.1. CO_2 solutions preparation

CO_2 solutions were prepared by dissolving the appropriate concentration of sodium carbonate in decarbonated and deaerated deionized water. Prior studies (not showed), confirmed that the pH of the sodium carbonate solution was always greater than 11, regardless of the concentration of sodium carbonate employed. This, according to the graph presented in Figure VI.5, in appendix VI.6, is most convenient as a pH ≥ 9.6 makes it possible to deaerate the solutions without losing any gaseous CO_2, as the predominant species are HCO_3^- and CO_3^{-2}. When the carbonate solution was introduced onto a more acidic environment, CO_2 becomes available in its gaseous form.

Throughout this work, the CO_2 concentrations presented do not take into account the atmospheric CO_2 that, despite decarbonation, may remain dissolved in the deionized water used to make the carbonate solutions employed in the kinetic assays, and assumes that at a pH of 6.8, CO_2 represents 19% of all carbonate species in solution.

II.7.2. Analysis of initial rate data

The initial reaction rates *versus* substrate concentration were plotted, and fitted using the Michaelis-Menten equation (equation II.1).

(equation II.1)

$$v_i = \frac{V_{max} \times [S]}{K_M + [S]}$$

Where v_i is the initial rate, [S] represents substrate concentration, and K_M is defined as the substrate concentration where v_i = ½ V_{max}. Kinetic parameters, K_M and V_{max} were calculated, using GraphPad Prism version 6.00 for Macintosh, by fitting of a theoretical curve to a Michaelis-Menten model employing a least squares fit.

To allow for a direct comparison, regardless of the concentration of enzyme employed in the assay, V_{max} was converted into turnover constant (k_{cat}) employing the equation presented below.

(equation II.2)

$$k_{cat} = \frac{V_{max}}{[Fdh]}$$

III. RESULTS AND DISCUSSION

III. RESULTS AND DISCUSSION

III.1. Cell growth optimization

In order to determine cell growth conditions that would allow for a greater cellular mass harvest and Fdh expression *D. desulfuricans* ATCC 27774 *(Dd*) cells were cultivated in anaerobic flasks containing different lactate-based media.

III.1.1. Medium type

A first screening was done to find the media that allowed for a higher cell mass to be harvested. This screening involved: ATCC 42, ATCC 1249, ATCC 2755, ATCC 27774, LSYC, VMN and M media. As media composition, presented in Appendix VI.1, is somehow similar in most cases, one would expect *Dd* cells to grow in all media with only slight different growth rates. However, a visual inspection of the flasks, after a 24-hour incubation period at 37ºC, demonstrated that in some media there was little propagation. The cells in these media were allowed to incubate for an additional 24h period, in total 48 hours, before another visual inspection was done. This screening resulted in the discarding of ATCC 42, ATCC 27774 and LSYC media, and the media that allowed for a greater cellular mass recovery of *Dd* cells, ATCC 1249, ATCC 2775, VMN and M were employed in a second screening.

The primary objective of this initial screening was to determine optimized conditions for the growth of *Dd* cells. As so, the reasons why some of the media did not allow the propagation of *Dd* cells were not studied at this time.

III.1.2. Gaseous phase

VMN, M, ATCC 1249 and ATCC 27774 were selected for further analysis to determine the best conditions for Fdh expression. Growths were performed under two different gas phases: argon and hydrogen since Silva, *et al*. (2001) [33] reported that growing *Desulfovibrio vulgaris* (*Dv*) under hydrogen led to a higher expression of Fdh

genes, an attempt was made to determine if this could also be the case for *Dd* cells. A first growth was made using solely VMN medium, as it was the medium that allowed for a greater recovery of *Dd* cells. This growth was done with an inoculum volume equal to 10% of the total growth volume and, after 24 hours, the cells were harvested by centrifugation. To determine Fdh activity within the periplasmatic extracts, in gel activity assays were performed. Following four freeze-thaw cycles the cells were centrifuged to obtain the periplasmatic soluble extracts. After electrophoretic separation, the activity assays were performed at room temperature under anaerobic conditions, by placing the gel in a Tris-HCl buffered solution at pH 8 containing sodium formate and β-mercaptoethanol. Activity bands developed after the addition of methyl viologen and were fixed with 2,3,5-thiphenyltetrazolium chloride. Figure III.1 shows the resulting PAGE activity gel. This gel, performed with equal concentrations of periplasmatic extract and a control consisting of pure Fdh, shows that cells grown in VMN under H_2 had less Fdh activity than those grown under an Ar gas phase.

Figure III.1 – In gel Fdh activity assay for *D. desulfuricans* ATCC 27774 soluble extracts grown in VMN medium under different gas phases. The amount of total proteins loaded in each lane was 78 μg. (Lanes: C – Fdh control, pure Fdh; 1 – *D. desulfuricans* grown under Ar; 2 – *D. desulfuricans* grown under H_2).

Nonetheless, as Fdh expression might be different in the other media, ATCC 1249, ATCC 27774 and M media, were also tested.

Growth in different media was evaluated by measuring O.D. values at 600 nm and by weighing the wet cell mass harvested after centrifugation following a 24-hour incubation period. These results, summarized in Table III-1, show that the O. D. value for cells grown under H_2 was approximately half of that measured for cells grown under Ar. In regard to the cell mass recovered, for ATCC 1249, ATCC 2775 and VMN media it follows the same trend as the O.D. value of cells grown under H_2 and is approximately half of that measured for cells grown under Ar. In M medium the harvested cell mass is roughly the same in the growths with H_2 and Ar gas phases. This discrepancy might be due to different growth rates for VMN, ATCC 1249 and ATCC 2755 media, depending on the gas phase that is employed. By opposition, *Dd* cells grown in M medium do not show a significant difference in growth rates regardless of the gas phase.

Table III-1 – Evaluation of cell growth in the various media used.

Medium	*VMN*		*ATCC 1249*		*ATCC 2755*		*M*	
Gas phase	Ar	H_2	Ar	H_2	Ar	H_2	Ar	H_2
O.D. $_{(600nm)}$	1.19	0.573	0.309	0.161	0.312	0.162	*	*
Wet weight (g)	0.794	0.553	0.641	0.290	0.553	0.241	0.419	0.483

* Medium composition does not allow for O.D. to be measured as an iron sulfide precipitate darkens the medium.

In gel activity assays from the extracts obtained of each media showed no Fdh activity for neither Ar nor H_2 grown cells. As no Fdh activity was found, it was hypothesized that these results could be due to inefficient freeze-thaw cycles resulting in Fdh not being extracted from the cellular fraction.

To test this hypothesis new growths were obtained in the same conditions, but to circumvent the possibility that the cell membrane was not being efficiently disrupted, both the periplasmatic and total soluble cellular fractions were prepared. After proceeding as described to obtain the periplasmatic soluble extracts, following centrifugation the cells were resuspended in 10 mM phosphate buffer (pH 7), and disrupted with a French Press at 20000 psi, and after centrifugation the cellular soluble extracts were obtained. Fdh activity was evaluated with an in gel activity assay, as

described above. This assay, whose results are depicted in Figure III.2, shows that Fdh activity is only present in cells grown under Ar in ATCC 2755 and VMN media and completely absent from the growths made under H_2.

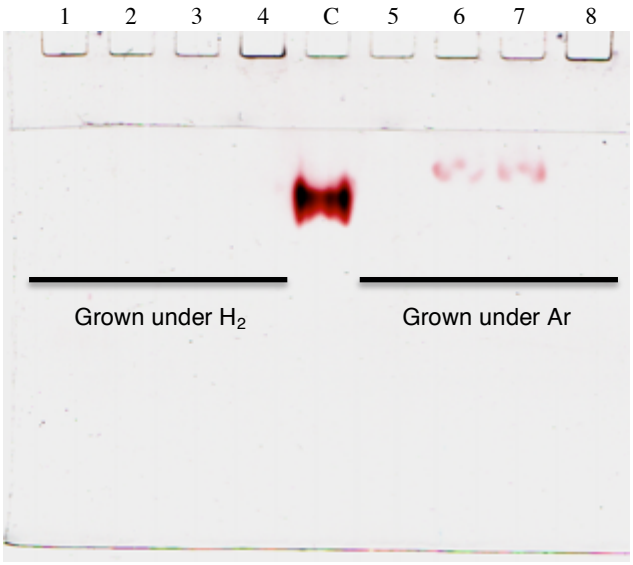

Figure III.2 – In gel Fdh activity assays for *D. desulfuricans* ATCC 27774 cells disrupted with a French Press after growing in different media and under different gas phases. The amount of total proteins loaded in each lane was 110 µg. (Lanes: 1 – ATCC 1249 medium; 2 – ATCC 2755 medium; 3 – VMN medium; 4 – M medium; C – Fdh positive control; 5 – ATCC 1249 medium; 6 – ATCC 2755 medium; 7 – VMN medium; 8 – M medium).

III.1.2.1. Gaseous phase influence in the pH of the media

As the growths performed under H_2 were not being as successful for *Dd* as those reported in the literature for *Dv*, following cell harvest, the pH values of the media were measured in an attempt to explain the results obtained.

Table III-2 shows the media pH values before inoculation ($pH_{initial}$) and after cell harvest (pH_{final}) and the observed pH variation (ΔpH). The table also shows the pH value variation between the final pH value of the media in the different gaseous phase employed (ΔpH_{gp}). These pH measurements show that, for growths made under H_2, the final pH of the media is more alkaline when compared to the final pH of the growths under Ar.

The pH variation ranges from -0.8 to +0.3 pH units in the Ar purged media, and from -0.3 to +1.8 pH units in the H_2 purged media. However, as no growth curve

relating *Dd* growth rates at different pH could be found during bibliographic research, one could only speculate if a change of 0.5 pH units, the smallest pH difference between the final pH of the Ar purged media and the H_2 purged media, is sufficient to hinder growth.

Table III-2 – Media pH value variations following cell harvest. pH values before inoculation ($pH_{initial}$) and after cell harvest (pH_{final}) and the observed pH variation (ΔpH) when compared with the initial pH value of the medium. ΔpH_{gp} represents the pH changes between the final pH value of the media in the different gaseous phase employed.

Medium	*VMN*		*ATCC 1249*		*ATCC 2755*		*M*	
Gas phase	Ar	H_2	Ar	H_2	Ar	H_2	Ar	H_2
$pH_{initial}$	7.5		7.5		7.8		7.5	
pH_{final}	7.8	9.3	7.1	8.0	7.0	7.5	7.7	8.5
ΔpH	+ 0.3	+ 1.8	- 0.4	+ 0.5	- 0.8	- 0.3	+ 0.2	+ 1.0
ΔpH_{gf}	+1.5		+0.9		+0.5		+0.8	

As the experimental setup employed to support the growths performed under an H_2 atmosphere did not allow for samples to be periodically taken, it was impossible to ascertain when in the growth stage these pH changes occur, and if they are in fact responsible for the poor results of the growths performed under H_2. To determine if pH changes are in fact responsible for the results obtained in growths performed under H_2 a new growth in a pH controlled reactor should have been executed. Another factor that may be responsible for the aforementioned results is the turbulence introduced by the flow of H_2 into the flasks. This hypothesis could be tested by also continuously flushing the control flasks with Ar. However, the experimental set up for argon flushing could not be set up during the course of this thesis.

According to the results described above, VMN medium under argon atmosphere was chosen to proceed with these studies. As M medium, displayed no Fdh activity after in gel activity assays it was discarded and subsequent tests were done solely with VMN medium.

III.1.3. Inoculum volume and growth stage harvest

The next step in the optimization of *Dd* cell growth and of Fdh expression was the evaluation of the growth curves of *Dd* cells and associated parameters.

A growth curve for *Dd* in VMN medium with a 2% inoculum is represented in Figure III.3. It follows the expected trend with an initial lag phase characterized by little or no bacterial growth, during which, *Dd* cells are adjusting to the environment and growing in size. This phase is followed by an exponential growth phase where *Dd* cells are in a rapidly growing and dividing state. During this phase *Dd* the cells reach a maximum growth rate. The time it takes for the bacteria to double in number during a specific time period is known as the doubling time. The third phase is the stationary phase. Throughout this phase growth levels are stable, due to the equilibrium between the rate of cell division and the rate of cell death. When this phase is reached most of the nutrients in the medium were consumed and the toxicity of the medium is high due to the accumulation of toxic metabolic waste products.

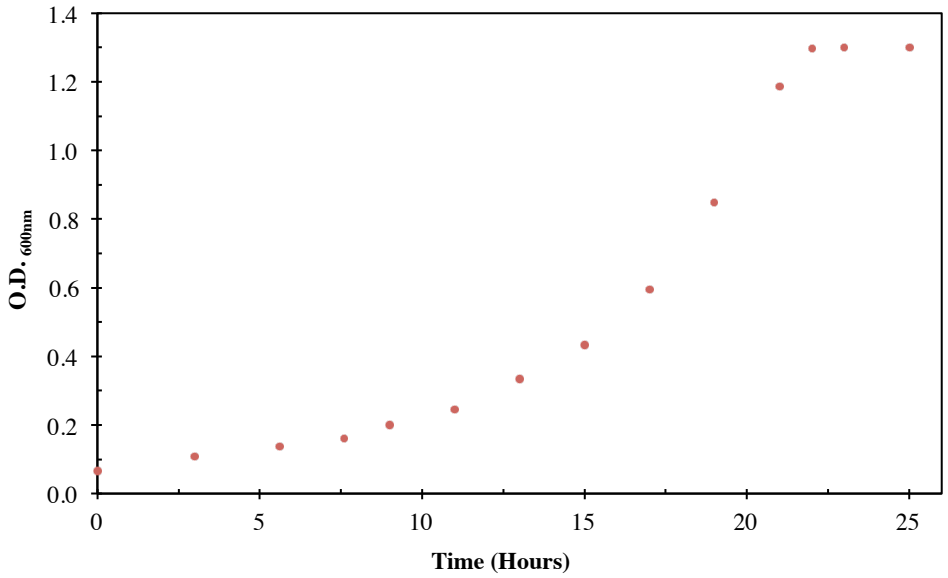

Figure III.3 – *D. desulfuricans* ATCC 27774 growth curve in VMN medium with a 2% inoculum.

The next tests were meant to determine how the amount of inoculum influenced the growth curve. This assessment allowed for a better understanding of the time scale involved in the different growth stages. Figure III.4 shows the different growth curves

and the fits used to calculate growth rate and doubling time, according to a model developed by Baranyi and Roberts [71].

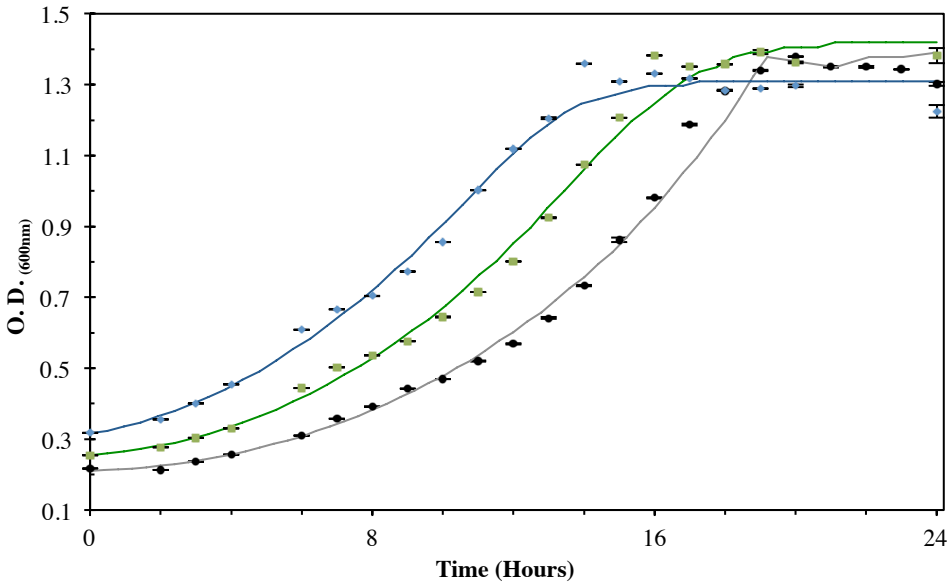

Figure III.4 – Effect of different inoculum volumes on *D. desulfuricans* ATCC 27774 growth curves in VMN medium and respective sigmoidal fits. Growth curves were made in triplicate. Experimental data are presented with the standard deviation. Experimental data: ● - 2% inoculum; ● - 5% inoculum; ● - 10% inoculum (total growth volume). Sigmoidal fit to experimental data for: **Grey** - 2% inoculum; **Green** - 5% inoculum; **Blue** - 10% inoculum.

Each of the three growth curves, presented above, follows the expected model for bacterial growth. There is an initial lag phase of very slow growth (*ca*. 3, 2 and 1h for a inoculum of 2, 5 or 10% of total growth volume, respectively). This initial phase is followed by a phase of exponential growth, up to 19, 17 and 15h, for an inoculum of 2, 5 or 10% of total growth volume, after which a stationary phase is reached.

The growth parameters determined: growth rate, doubling and lag time, as well as the adjust quality of the theoretical model to the experimental data are summarized in Table III-3.

Table III-3 – Growth parameters and model fit convergence quality descriptors for *D. desulfuricans* ATCC 27774 in VMN medium, using different inoculum volumes.

Inoculum volume	Growth rate (h^{-1})	Doubling time (h)	Lag time (h)	Convergence	
				R^2	SE of fit
2%	0.121 ± 0.005	5.86	3.26 ± 0.54	0.99	0.05
5%	0.122 ± 0.005	5.95	1.99 ± 0.54	0.99	0.05
10%	0.120 ± 0.005	6.01	1.12 ± 0.52	0.99	0.04

As expected, the growth rates and doubling times are very similar between the growths with different inoculum volumes. The inoculum volume only affects the duration of the lag phase, as these are greater when the inoculum volume is smaller.

Attending to restrictions imposed by the laboratory that was going to scale up the growth volume, the following studies were done using 2 and 10% inoculums. These allowed for mid exponential phase to be reached in 10 or 15 hours, if a 10 or 2% inoculum was used, and for the cells to be in a stationary phase after 15 or 20 hours if an inoculum of 10 or 2% were employed.

After the selection of the growth media, gaseous phase and optimization of inoculum volumes, the goal was to determine if *Dd* Fdh expression was influenced by harvesting it at different growth stages, mid exponential growth phase and at the stationary phase. Growths were performed in VMN medium as in the previous study and cellular soluble extracts were obtained. Table III-4 accounts for the O.D. value and wet weight of cells harvested of growths with different inoculum volumes and evaluated at different growth stages (mid exponential and stationary).

Table III-4 – Influence of the use of different inoculum volumes and cell harvest at different growth stages in a 100 mL growth.

Medium	*VMN*			
Growth stage	mid exponential		stationary	
Inoculum volume	2%	10%	2%	10%
O.D. $_{600\ nm}$	0.841	0.946	1.336	1.311
Wet weight (g)	0.514	0.564	0.892	0.784

Fdh activity was assessed employing in gel activity assays. These results, depicted in Figure III.5, show no significant difference in band intensity for VMN grown cells regardless of the inoculum volume employed, 2 or 10%, and of the growth stage where the cells were harvested, mid exponential or stationary phases.

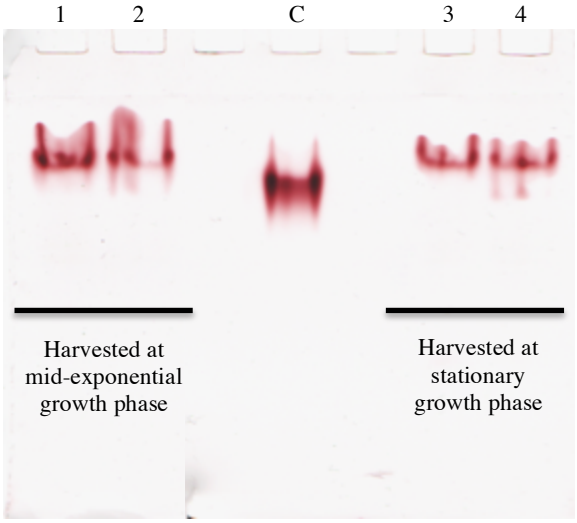

Figure III.5 – Effect of inoculum volume and different growth stage harvesting in *D. desulfuricans* ATCC 2774 Fdh expression. In gel activity assays for cells grown with 2 or 10% inoculum volume and disrupted with a French Press after harvesting either after mid-exponential phase or after 24 hours. The amount of total proteins loaded in each lane was 159 µg. (Lanes: 1 – VMN medium, 2% inoculum; 2 – VMN medium, 10% inoculum; C – Pure Fdh control; 3 – VMN medium, 2% inoculum; 4 – VMN medium, 10% inoculum).

In the literature it is described that the addition of a reductant is required to maintain Fdh active [72]. To understand if a reducing environment would yield a significant difference in active Fdh harvested, 1 mM of a common reducing agent, DTT, was added to the cell ressuspension buffer. Additionally, 1mM PMSF, a serine protease inhibitor, was also employed during cell disruption in an effort to keep enzymatic degradation of Fdh to a minimum. For *Dd* cells grown in VMN, Fdh activity in gel, whose results are presented in Figure III.6 do not show, as expected, significant differences regardless of inoculum volume. This meant that no apparent difference existed between using 2 or 10% of inoculum as long as the cells were harvested at the same growth stage. Figure III.6 shows that the highest Fdh activity is found in samples that were harvested after a 24-hour incubation time. These results can be due to a depletion of nutrients or waste accumulation in the medium might have lead to the

activation of a different metabolic pathway that requires Fdh, thus making way for an augmentation of its gene expression. Regarding the addition of DTT and PMSF to the ressuspension buffer, prior to cell disruption, results show no noticeable effect when samples are harvested after 24 hours whatever the amount of inoculum. However, for samples harvested at mid-exponential phase, addition of DTT and PMSF appears to have a positive effect in maintaining Fdh activity. As abovementioned, the samples derived from this growth stage have less Fdh activity, when compared to samples harvested after 24 hours of growth, so it is fair to assume that inhibiting serine proteases helps to keep active the small concentration of Fdh that exists in the extract.

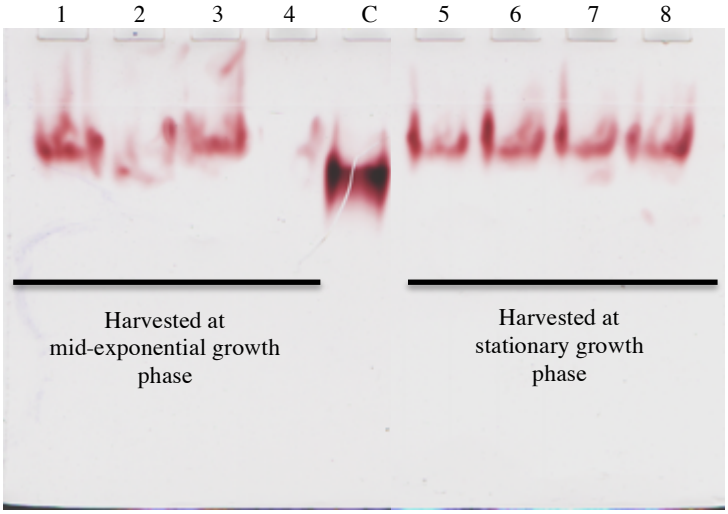

Figure III.6 – Effect of inoculum volume, different growth stage harvesting and the presence or absence of PMSF and DTT in the expression of *D. desulfuricans* ATCC 27774 Fdh. In gel activity assay for cells grown in VMN medium with inoculums of 2 or 10% (of the total growth volume), harvested either after mid-exponential phase or after 24 hours and disrupted with a French Press in the presence (w) or absence (w/o) of PMSF and DTT. The amount of total proteins loaded in each lane was 159 μg. (Lanes: 1 – VMN medium, 2% inoculum (w); 2 – VMN medium, 2% inoculum (w/o); 3 – VMN medium, 10% inoculum (w); 4 – VMN medium, 10% inoculum (w/o); C – Pure Fdh positive control; 5 – VMN medium, 2% inoculum (w); 6 – VMN medium, 2% inoculum (w/o); 7 – VMN medium, 10% inoculum (w); 8 – VMN medium, 10% inoculum (w/o)).

However, as the results depicted above do not show a clear trend in relation to the benefits of DTT and PSMF addition it was reasoned to choose the growth conditions that allowed for a higher cell mass harvest. VMN was chosen as the medium to use for the scale-up process and based on the results above, growth conditions were defined as follows:

Table III-5 - Growth condition for scale-up process.

Medium	*VMN*
Inoculum (of total volume growth)	2%
Growth stage harvest	stationary (20 hours)

III.2. Fdh purification

As a large quantity of pure Fdh was necessary for carrying out the kinetic assays and no overexpression protocol exists, to obtain sufficient protein it was necessary to resort to large reactors, making it necessary to outsource a 200 L cell growth. This growth was made according to the conditions defined in Table III-5, yielding 170 g cell, wet weight, corresponding to 0.85 g cells/liter of culture medium, as opposed to an average of 7 g cells/liter of culture medium obtained in the growths made in the 100 mL flasks, and the 5 g cells/liter of culture medium from previous growths made employing a 300 L reactor under the same conditions [73].

In spite of the low yield obtained, it was decided to initiate the purification procedure. Cells were disrupted with a high-pressure homogenizer at 9000 psi. Following centrifugation, to remove cell debris, and ultracentrifugation, to remove membranes, the crude extract was fractionated by anion exchange chromatography, using a DEAE Bio Gel (25x ø4.7 cm), equilibrated with 10 mM Tris-HCl. After a washing step, the elution was accomplished with a linear gradient, 10 to 300 mM Tris-HCl, in 3 column volumes and, as depicted in Figure III.7, nine fractions (F1-F9), were collected. The Fdh activity in each fraction was assessed by PAGE activity assays and protein content by SDS-PAGE (Figure III.8), both in 7.5% polyacrylamide gels.

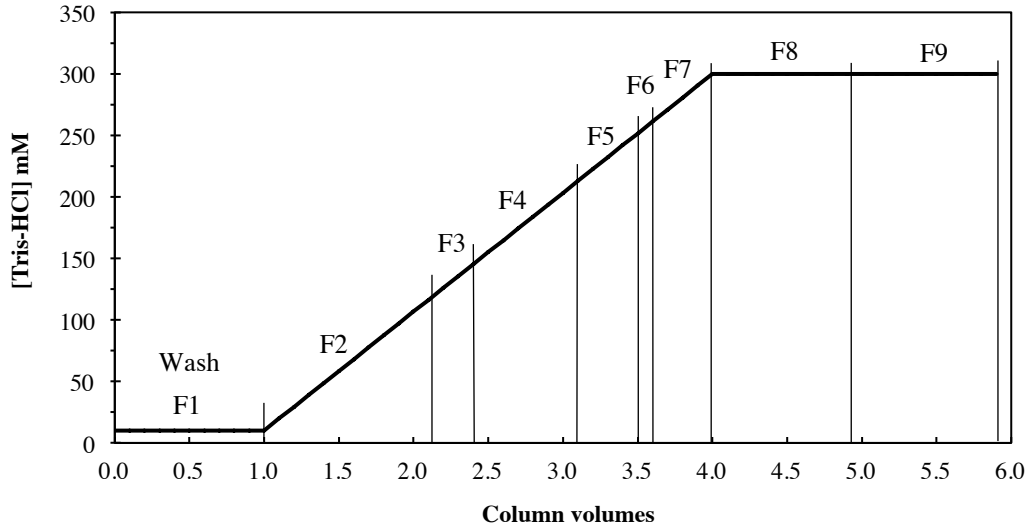

Figure III.7 – Crude extract fractionation on an anion exchange chromatography, DEAE Bio Gel equilibrated with 10 mM Tris-HCl. F1—F9 represent each of the factions collected. Column volume was approximately 440 mL.

Figure III.8 shows the SDS-PAGE gel of the fractions from this first chromatographic step. The arrows indicate where Fdh subunits (88, 29 and 16 kDa) are expected based on subunit apparent molecular mass.

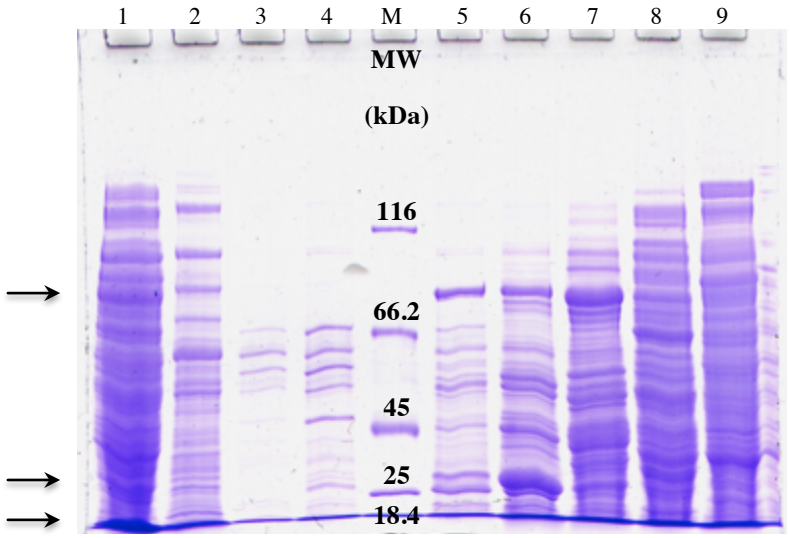

Figure III.8 – SDS-PAGE from the fractions collected after the first chromatographic step; 20 µL of each sample were loaded into each lane of a 7.5% polyacrylamide gel. (Lanes: 1 – Total soluble fraction; 2 – F1; 3 – F2; 4 – F3; M – Fermentas unstained molecular weigh protein marker; 5 – F4; 6 – F5; 7 – F6; 8 – F7; 9 – F8).

To evaluate Fdh activity within each fraction a native 7.5% polyacrylamide gel was loaded with the same fractions as the SDS polyacrylamide gel and pure Fdh to perform an in gel Fdh activity assay. Although the gel presented in Figure III.8 shows in lanes 5 and 6, three large bands compatible with the molecular weight of the three subunits that compose *Dd* Fdh, in gel Fdh activity assays did not show activity for any of the collected fractions. This can be due to the recovering of an inactive form of Fdh or simply to the presence of other proteins with the same molecular weight.

As this was an outsource growth, limited information is available to explain the low yield of harvested cells and the inexistence of Fdh within the crude extract.

As no active Fdh was present in the cells, subsequent purification procedures were not performed and preliminary assays and steady-state kinetics were done using a frozen enzyme batch that was previously purified in the laboratory.

III.3. Preliminary kinetic studies

The formate oxidation reaction catalyzed by Fdh requires the addition of a mediator that will act as a terminal accepter of the two electrons resultant from the oxidation of formate according to the scheme presented below.

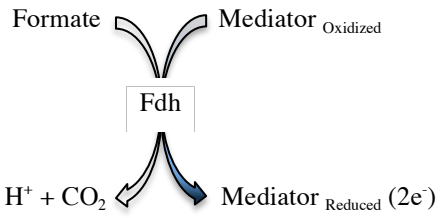

Figure III.9 – Schematic representation of the formate oxidation reaction, catalyzed by Fdh in the presence of a mediator. In these assays the mediator employed was benzyl viologen. When oxidized benzyl viologen is colorless and when it is reduced it turns blue as depicted in the arrow on the right.

Throughout these studies the mediators employed belong a class of compounds derived from 4,4'-bipyridyl known as viologens. These compounds have been extensively used in chemical and biochemical studies as oxidation-reduction indicators due to their reduction to the radical mono cation being colored intensely blue.

III.3.1. Triggering the enzymatic reaction

To characterize the formate oxidation reaction catalyzed by Fdh two different assays methods were employed. In the first method, the formate oxidation reaction was triggered by the addition of the substrate (formate) [65], whereas in a second method Fdh was incubated with formate before the reaction was initiated by the addition of mediator [74]. Both assays employed a large concentration of a sulfhydryl reducing agent, β-mercaptoethanol, in the mM range, while using enzyme concentrations in the nM range.

Two timecourses are presented in Figure III.10, one where Fdh was previously incubated with formate (red line) and another where there was no incubation with formate (black line).

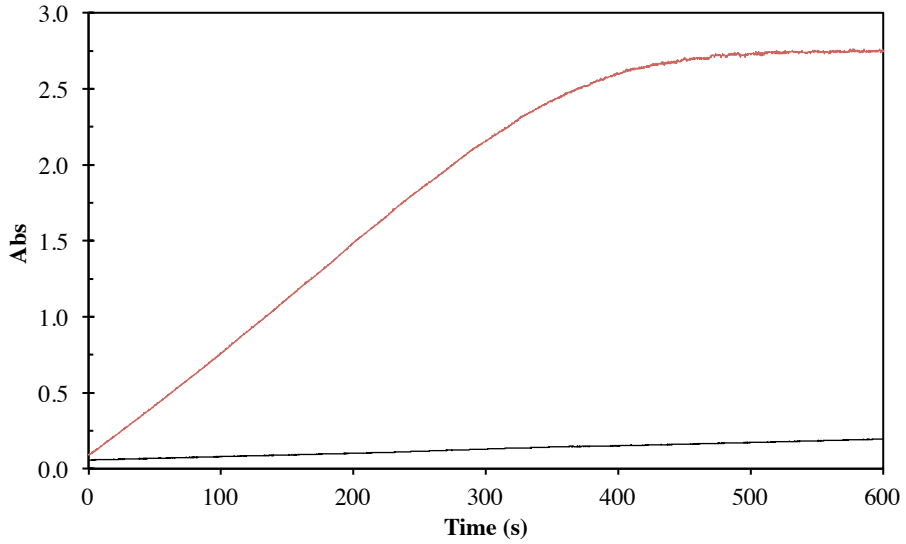

Figure III.10 – *D. desulfuricans* ATCC 27774 Fdh timecourses for formate oxidation, with or without the activation procedure. Timecourses of the reduction of benzyl viologen monitored at 555 nm; Fdh (4 nM) in 60 mM Tris-HCl pH 8.0 and 133 mM β-mercaptoetanol. **Red**: with activation: Fdh was incubated with 140 μM sodium formate and the reaction was started adding 7.5 mM benzyl viologen; **Black**: without activation: reaction was started with the addition of 140 μM sodium formate. The assays were performed under an argon atmosphere in stoppered quartz cells.

These results show that a higher initial reaction rate is obtained when the enzyme was first incubated with formate (red line). Moreover when such incubation does not occur (black line) the assay presents an initial lag phase with almost null initial rate. Taken together these results indicate that the enzyme needs to be activated by incubation with formate in order to initiate the catalytic cycle.

A set of preliminary assays was performed to better understand the oxidation/reduction processes that occur during steady-state kinetic assays, in particular with regard to the role of the sulfhydryl reduction agent. However, due to its chemical instability and hazardous effects on human health, β-mercaptoethanol was, in this work, replaced by dithiothreitol (DTT), chemically more stable and less volatile.

These studies also allowed for a better understanding of how the oxidation state of the enzyme influences the formate oxidation reaction. Enabling us to define the succession of additions and ensure the best method was chosen to perform the steady-state kinetic assays.

To understand if the sulfhydryl reducing agent, DTT, was necessary to change the oxidation state of the enzyme its reduction was followed by visible spectroscopy 300-700 nm (60 mM Tris-HCl pH 8 and 0.8 μM Fdh) under anaerobic conditions. Fdh spectrum displays a typical cytochrome *c* spectrum with characteristic features as Soret, α and β bands dominating the spectra in the reduced species. So, most of the information conveyed regards the oxidation state of the hemes that are part of the electron transfer pathway of the enzyme, that also includes two [4Fe-4S] clusters, as stated in Section I.4.1.1. The spectra in Figure III.11 shows that the addition of DTT reduces the hemes and a spectrum with the characteristics of the reduced species arises. The oxidized species (green line) exhibits an absorption maximum at 409 nm (Soret) and a large band centered at 527 nm. While in the DTT-treated Fdh spectra, α and β bands are visible at 523 and 552 nm, respectively, and the Soret (γ) band shifts from 409 to 419 nm. Subsequent timecourses showed that the α and β bands start to fade and the Soret band changes its center to a wavelength in between that of the reduced and oxidized species. This trend is illustrated in the spectrum by the direction of the arrows and shows that an incomplete reduction is achieved with the addition of DTT as the spectrum obtained after DTT addition displays characteristics of both, the reduced and the oxidized species. These two populations comprise reduced and oxidised Fdh resulting in a spectrum with mixed characteristics as the one presented in Figure III.11. Although DTT is a strong reducing agent, with a standard reduction potential of -327 mV at pH 7, its reducing power is limited at the pH these assays were done (pH 8) [75]. This is due to the reactivity of a dithiol being influenced by the lower pKa of the two thiols. For DTT the pKa values of its dithiols are 9.2 and 10.1. Therefore, at pH 8 the majority of the thiol groups are in an inactive protonated form. This limitation was addressed by employing a stoichiometric proportion between DTT and Fdh of approximately 60:1, to ensure that the proportion of molecules in a reactive thiolate form is enough to interact with all Fdh present in the assay. However, as this assay gave rise to two populations it suggests that other modifications may occur that influence the electron transfer pathway. This supposition can be verified in future studies, e.g., EPR studies, that probe the metal centers involved.

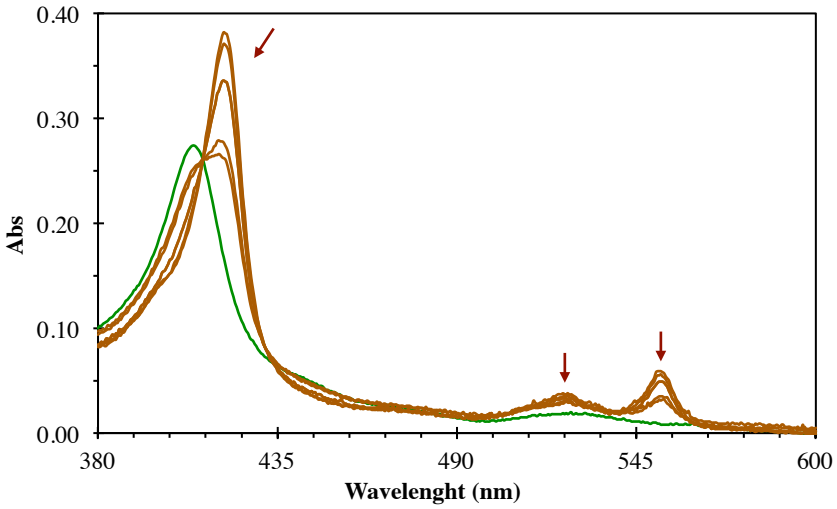

Figure III.11 – Fdh spectra, as purified and evolution after DTT addition. Spectra were obtained employing a reaction mixture composed by 60 mM Tris-HCl pH 8 and 0.8 µM Fdh. **Green**: Fdh spectra as purified, oxidized; **Brown**: Fdh spectra evolution after a 50 µM DTT addition. The time elapsed between the acquisition of each spectrum was approximately 2 minutes. The direction of the arrows represents the spectra trend after DTT addition.

Costa, *et al*. (1997) [65], described that the addition of a sulfhydryl reducing agent to the reaction mix was essential to eliminate the lag phase. In the studies shown above it was possible to verify that the sulfhydryl reducing agent reduces the electron transfer pathway of Fdh. Thus, suggesting that its addition is necessary to reduce the enzyme prior to the beginning of a catalytic cycle, and thus yield a higher initial rate.

Besides the sulfhydryl reduction agent, Mota, *et al*. (2011) [74] also indicate that it is important to incubate Fdh with formate before triggering the oxidation of formate. This being the case, to know how formate influenced the oxidation state of Fdh, after DTT addition formate was also added to the reaction mixture. As shown in Figure III.12, after the addition of 83 µM formate (red line), the DTT-treated Fdh spectrum originated is compatible with that of the reduced species, with well defined α and β, and a sharp Soret band centered at 419 nm with an additional shoulder centered around 400 nm due to the reduction of the [4Fe-4S] cluster [74].

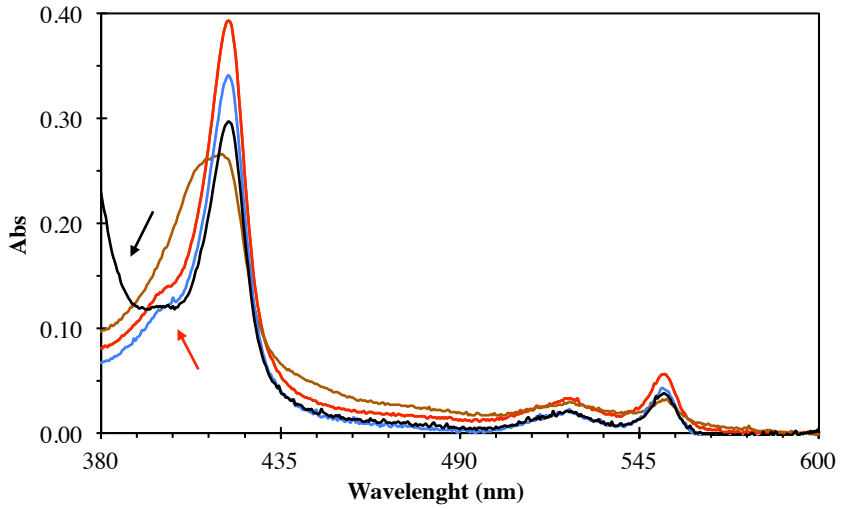

Figure III.12 – DTT-treated Fdh spectra and after the additions of 83 and 230 µM sodium formate. Brown: Fdh spectrum after DTT addition, as in Figure III.11; **Red**: Fdh spectrum after addition of 83 µM sodium formate. **Blue**: Fdh spectrum after the addition of 230 µM sodium formate. **Black**: Fdh spectra after sodium dithionite addition. The black arrow points the dithionite spectrum superimposition with that of Fdh and the red arrow points the shoulder that arises at 400 nm after formate addition due to the reduction of the [4Fe-4S] cluster.

Further additions up to 230 µM sodium formate (Figure III.12, blue line) have no effect on the spectra (the lower absorbance in Figure III.12 is a result of the dilution effect). An addition of sodium dithionite (Figure III.12, black line), a strong reductant with a standard reduction potential of -660 mV at pH 7 [76], was done and also had no influence on the spectrum, other than the appearance of an enlarged band below 390 nm (Figure III.12, black arrow).

In Figure III.12, as the Soret band dominates the spectrum, only a shoulder of the [4Fe-4S] clusters is visible, at 400 nm (red arrow) after the addition of formate, hinting that only formate has the ability to reduce them. Furthermore, after the hemes are reduced with the first formate addition subsequent formate and dithionite additions have no effect on their oxidation state. This suggests the activation depicted in Figure III.10 might be related to reaction mechanism proposed by Mota, *et al*. (2011) [66] and Cerqueira, *et al*. (2013) [77]. They proposed that a rearrangement mechanism, named sulfur-shift, depicted in Figure I.18, allows the enzyme to shift between active and inactive forms by allowing or blocking substrate binding to the Mo (VI) ion in the active site, by displacement of a selenium atom, opening a coordination position where

formate can bind directly to the Mo (VI) ion. The results presented in Figure III.10, support this mechanism as only the Fdh incubated with formate, prior to initiation of the assay, yielded a high initial rate for the formate oxidation reaction.

In conclusion the assays described above showed that the complete reduction and activation of Fdh could only be obtained in the presence of formate. This way, in all subsequent assays the kinetic reaction was initiated by addition of the mediator instead of formate. As for the sulfhydryl reduction agent, although its interaction mechanism with the enzyme is unknown it is thought that it is needed to remove O_2 in the enzymatic assay and also to decrease the redox potential of the system [65,72].

III.3.2. The role of the sulfhydryl reducing agent

All kinetic assays described in the literature employ high concentrations of a sulfhydryl reducing agent, usually β-mercaptoethanol. Although the mechanism of interaction between the enzyme and the sulfhydryl reducing agent is still unclear, it seemed odd that to activate enzyme concentrations in the nM range, mM of a sulfhydryl reducing agent were needed. Subsequently, the effect the sulfhydryl reducing agent had on the initial rates was studied for different formate and DTT concentrations.

Due to the limited amount of enzyme available during the course of this thesis only a few experiments could be performed. These assays were done, in triplicate, with 0, 2 or 100 mM DTT and formate concentrations ranging from 70 μM to 5 mM. Table III-6 summarizes the results obtained. These showed that DTT only affected the reaction rates when low concentrations of formate were used (μM range) and that reaction rates lowered with the increase of DTT concentration.

Table III-6 – Influence of DTT concentration on formate oxidation initial rates. Fdh (5 nM) in 60 mM Tris-HCl pH 8.0. Fdh was incubated with formate and DTT for 30 minutes under anaerobic conditions. The reaction was started with the addition of 7.5 mM benzyl viologen and the assays were performed in triplicate, under an argon atmosphere in rubber stoppered quartz cells. For each formate concentration used, the mean of the initial rates and its standard deviation are summarized.

	$v_i (\mu M.min^{-1})$		
	[DTT]		
[Sodium Formate]	0	2 mM	100 mM
70 μM	25.3 ± 0.4	22 ± 3	-
140 μM	32.9 ± 0.5	29 ± 1	4.7 ± 0.5
1 mM	-	38.2 ± 0.9	36 ± 2
5 mM	42 ± 1	42 ± 3	45 ± 2

These assays also showed that initial rates were not affected when sodium formate concentrations were in the milimolar range. Thus, according to the results described above it was decided that no sulfhydryl reducing agent would be used. This allowed for higher differences in absorbance to be recorded, making it easier to determine initial rates while also reducing the error committed in their determination.

III.3.3. Atmospheric O_2 interference in the kinetic assays

For an assay to be valid it should start without a lag period. If a lag period is observed, previous studies [64,65,72] attributed it to the presence of oxygen in the reaction mixture. It is thought that the sulfhydryl reducing agent plays a role in the removal of atmospheric oxygen from the assay, and that its presence, even in small concentrations, dramatically inhibits the enzymatic reaction [65]. However, the reaction mixture employed did not contain a sulfhydryl reducing agent. So, to replace it and account for the presence of oxygen in the argon being used to deaerate the system, an oxygen trap (Chemical Research Supplies) was placed in the deaeration line.

After this change to the experimental setup, the number of successful assays, without a lag phase after the addition of the mediator, did not differ from that that was obtained when a sulfhydryl reducing agent was added to the reaction mixture. Neither did it substantially differ from the number of successful assays done without both, the

sulfhydryl reducing agent and the oxygen trap. This suggests that the presence of trace amounts of oxygen might not be the sole cause of these lag phases. Cerqueira *et al*. (2013) attributed these lags to a rearrange of the catalytic center of the enzyme prior to its activation, the sulfur shift [77]. However, as for assays done under the same conditions the duration of these lags varies between a few seconds to dozens of minutes, there might be another factor that accounts for them other than the presence of oxygen or the sulfur shift. Nonetheless, the limited amount of Fdh available to perform formate oxidation assays prevented further experiences that could explain this behavior, from being done.

Additionally, it was found that the presence of oxygen only inhibits enzymatic activity if it is present prior to the beginning of the kinetic assay. After the catalytic cycle is initiated the quartz cell can be opened and the reaction mixture can even be transferred to another vial without any loss of enzymatic activity. This was observed in different conditions, with varying concentrations of either enzyme or substrate. After a kinetic assay, the quartz cell could be opened and the blue colored reduced mediator, benzyl viologen, resultant from the oxidation of formate to carbon dioxide, persisted in some cases for several hours, regardless of the atmospheric oxygen. This observation may suggest that if oxygen is present while the enzyme is incubating with formate the activation depicted in Figure III.10 does not occur and that once it happens oxygen can no longer interfere with the reaction.

III.4. Steady-state kinetic studies

III.4.1. Formate oxidation studies

The kinetic parameters for the formate oxidation reaction by Fdh were determined and compared with the ones previously reported by Mota, *et al*. (2011) [66] and with those reported for formate dehydrogenases isolated from different organisms.

The initial rates of Fdh reaction were calculated from the changes in absorbance over time due to the reduction of the mediator, benzyl viologen.

For each formate concentration the results were obtained in quadruplicate. As represented in Figure III.13, in the presence of varying formate concentrations the Fdh activity follows a Michaelis-Menten profile.

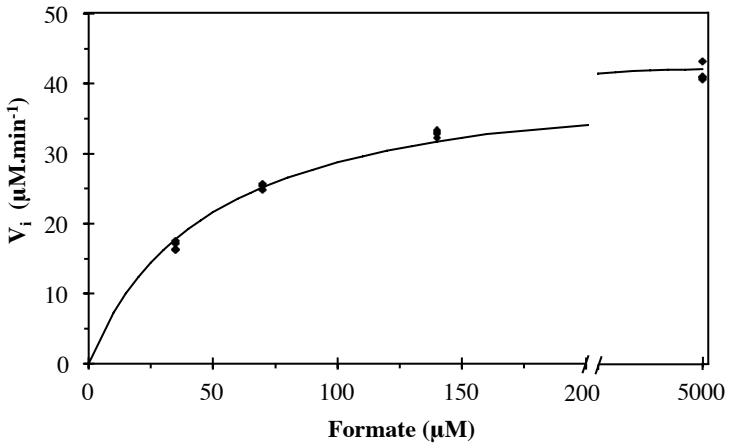

Figure III.13 – Kinetics of formate oxidation catalyzed by *D. desulfuricans* ATCC 27774 Fdh (♦). The initial rates of formate oxidation were measured by monitoring the reduction of the mediator, benzyl viologen, in 60 mM Tris-HCl buffer pH 8, catalyzed by 5 nM Fdh. **Line**: fitting of the experimental data to a Michaelis-Menten equation with kinetic parameters K_M = 49 µM and V_{max} = 43 µM.min^{-1}.

The kinetic parameters, V_{max} and K_M, determined by least square fitting of the experimental data to a Michaelis-Menten equation, are presented in Table III-7 together with the kinetic parameters determined for Fdhs isolated from other organisms.

Table III-7 – Comparison between kinetic parameters, k_{cat}, K_M and catalytic efficiency for formate oxidation catalyzed by formate dehydrogenases isolated from different organisms in the presence of benzyl viologen at pH 8.

	k_{cat} (s^{-1})	K_M (μM)	k_{cat}/K_M	Reference
Mo-Fdh *D. desulfuricans* ATCC 27774	146 ± 2	49 ± 2	2.97	This Work
	347	64	5.42	[66]
W-Fdh *D. gigas*	174	51	3.41	[66]
W-Fdh *Desulfovibrio alaskensis*	241	10	24.1	[66]
Mo-Fdh H *Escherichia coli* K12[§]	2833	$26x10^3$	0.11	[78]
W-Fdh *Syntrophobacter fumaroxidans* Fdh 1	4083	40	102	[72]
W-Fdh *Syntrophobacter fumaroxidans* Fdh 2	5625	10	563	[72]
NADH-Mo-Fdh *Rhodobacter capsulatus*[*]	36.5	281	0.13	[79]
NADH-W-Fdh *Clostridium carboxidivorans*[*]	6.30	70	0.09	[80]

[*] The mediator employed in these assays was NAD^+. [§]Assays performed at pH 7.5.

Table III-7, shows the catalytic efficiency of formate oxidation varies widely among the formate dehydrogenases isolated from different species and it is also evident that NAD^+-dependent Fdhs, regardless of the metal content of their active site, have a much lower catalytic efficiency when compared to NAD^+-independent Fdhs. These differences might be explained by the amino acid variability in the substrate binding pocket, which are thought to allow the tuning of the metal properties, influenced by the role the different enzymes play in each organism, to catalyze this reaction [39]. For instance, the Fdh isolated from *Clostridium carboxidivorans* displays the lowest catalytic efficiency for the formate oxidation reaction. This can be due to the metabolic role this Fdh has on this organism. As it is employed in a metabolic pathway leading to the fixation of carbon dioxide, this Fdh should be fine-tuned to perform the reduction of carbon dioxide [72]. Curiously, the propionate-oxidizing bacterium *Syntrophobacter fumaroxidans* needs two different W-Fdhs with a high catalytic efficiency. Fdh 2 has a catalytic efficiency five times higher than Fdh 1, hinting it might be the primary catalyst for formate oxidation while the other, although also able to perform the same reaction might be involved other processes. Nevertheless, for the Mo/W-Fdhs isolated from *Desulfovibrio* species, the turnover constants determined are in the same order of magnitude, suggesting the enzyme as whole, rather than the metal that comprises the active site is responsible for the specificity and turnover constant. Other studies also

support the supposition that the enzyme as a whole (amino acid residues and the other redox cofactors) is tailored to complement the metal and fine-tune the reduction potential of the active site. An example of this rises from the fact that if the molybdenum in the cofactor of a molybdenum-containing enzyme is exchanged for tungsten, the enzyme experiences a considerable loss of activity [39].

With exception to the K_M of the Mo-Fdh from *E. coli* K12 and that of NADH-Mo-Fdh from *R.* capsulatus, all others are quite similar. In *E. coli* K12 this difference can be explained by the presence of azide, a strong inhibitor, in the preparations used by Axley, *et al.* (2001) [66,78]. The turnover constant determined for the Mo-Fdh of *D. desulfuricans*, although within the same order of magnitude, it is roughly half of that determined by Mota, *et al.* (2011) [66]. Within the experimental error, one might suggest that the enzyme concentration might have been overestimated or that only half of the enzyme is in an active form. This might have been due either to the existence of inactive enzyme molecules within the batch or to an inaccurate determination of its concentration. As for the K_M, the value determined is similar to the one determined by Mota, *et al.* (2011) [66].

III.4.2. Carbon dioxide reduction studies

To reduce carbon dioxide it is necessary to have the mediator in a reduced state as depicted in Figure III.14.

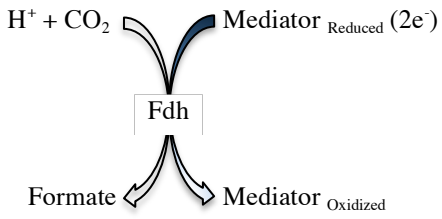

Figure III.14 – Schematic representation of the carbon dioxide reduction reaction, catalyzed by Fdh in the presence of a mediator. In these assays two mediators were employed, benzyl and methyl viologen. When reduced to the radical mono cation, these mediators are colored blue, but when oxidized turn colorless as depicted in the arrow on the right.

Before attempting to perform steady-state carbon dioxide reduction kinetic assays it was necessary to find a way to reduce and maintain the mediator reduced. In this work, the reduction agents used were dithionite and zinc pellets. However, due to the low standard reduction potential, characteristic of viologens, keeping them reduced was proving to be a challenge. So, a preliminary assay was done were the formate oxidation reaction was used as a source of reduced mediator. These experiments, depicted in Figure III.15, were steady-state kinetic formate oxidation assays, where sodium carbonate (CO_2 source) and/or water were added after the formate oxidation reaction reached equilibrium.

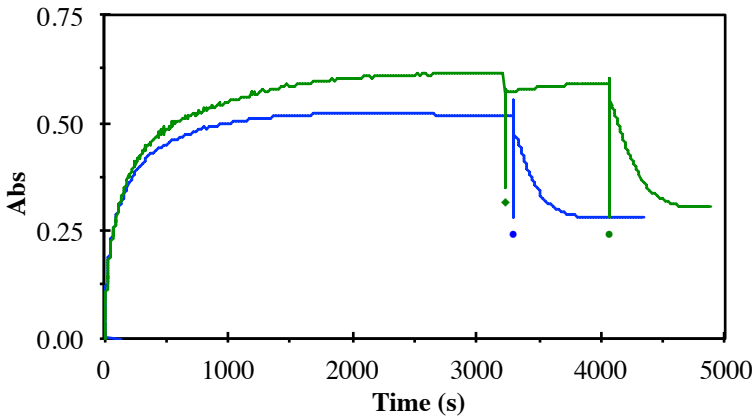

Figure III.15 – Mediator reduction timecourse in the presence of formate and its re-oxidation after sodium carbonate addition. Reaction was started with the addition of 625 µM benzyl viologen to a reaction mixture containing 15 nM Fdh in 100 mM Tris-HCl pH 8.0, 5 mM sodium formate. After reaching equilibrium a single addition (•) of 5 mM sodium carbonate was done (blue assay). In the green assay a first addition of deaerated H_2O was done (◆), as control, and subsequently an addition of sodium carbonate was performed (•). These assays were performed under an argon atmosphere in stoppered quartz cells by monitoring absorbance variations at 555 nm.

These assays show that after formate addition, to the reaction mixture containing Fdh, the mediator is quickly reduced and that after equilibrium is reached (*ca*. 30 minutes) the reduction level, determined by monitoring the absorbance variation at 555 nm, is stable. The subsequent carbonate addition induces a rapid and pronounced decay in absorbance that is related to the oxidation of the mediator. Thus suggesting that these results are due to the reduction of carbon dioxide, produced by the addition of carbonate to the reaction mixture, to formate. A control assay was performed where deaerated water was added to the reaction mixture before the addition of the carbonate solution,

since residual oxygen introduced upon addition of carbonate could also induce mediator reoxidation. As Figure III.15 shows, the addition of water (◆) had no effect on the reduction level of the mediator, further supporting that the carbon dioxide reduction is, in fact, occurring.

After this preliminary assay, showing the enzyme is able to catalyze carbon dioxide reduction, it was necessary to find a way to maintain the viologen, methyl or benzyl, reduced before being added to the assay. This led to the use of sodium dithionite to reduce the viologen. However, this method proved to be unreliable as the concentration of dithionite needed to completely reduced the viologen in the reaction mixture varied significantly. Furthermore, subsequent assays showed this reducing agent is able to interact with Fdh and the mediator, either methyl or benzyl viologen, rendering it impossible to determine the initial rates for this reaction, as can be observed in Figure III.16.

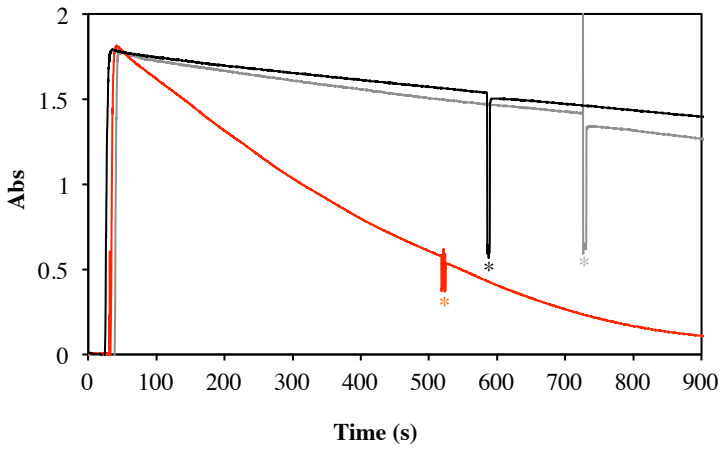

Figure III.16 – Interaction of sodium dithionite with Fdh in the presence of methyl viologen. **Black**: Control, no Fdh; **Grey**: 25 nM Fdh, denatured after 10 minutes at 100ºC; **Red**: 25 nM active Fdh. Reaction progress monitored at 607 nm. Reaction mixture contained 100 mM phosphate buffer pH 6.5 and 625 µM methyl viologen. Additions of 5 mM sodium carbonate are marked with (*). The assays were performed under an argon atmosphere in stoppered quartz cells.

The time courses depicted above show that after sodium dithionite addition there is an immediate absorbance increase that in all assays reaches roughly the same maximum due to the reduction of the mediator. After this maximum is reached, absorbance starts to decrease. This decrease rate is similar in the assays where no Fdh or

denatured Fdh was used, black and grey lines, respectively, and is significantly larger in the assay where active Fdh was employed, red line. After carbonate addition (*, *, *), none of the time courses exhibits a significant change to its absorbance decrease trend. The use of denatured enzyme demonstrated that active Fdh was responsible for the oxidation of the mediator, thus for the marked decrease in absorbance. These assays showed that the interaction between Fdh and the dithionite was in fact responsible for the oxidation of the mediator. This made it impossible to maintain a low and stable rate of absorbance decrease. Therefore this system could not provide the necessary sensibility to measure the absorbance variations that would arise from the oxidation of the mediator and concomitant reduction of carbon dioxide to formate. This was unexpected but during the course of this work there was no time to study the mechanisms involved in this reaction.

As this system did not prove to be reliable, it was necessary to develop one that did not interact with Fdh and that was able to completely reduce the mediator. The difficulty in preparing this mediator solution lies in the fact that by applying too strong a reducing agent there is the possibility for the occurrence of over-reduction. Over-reduction happens when a benzyl viologen molecule donates two electrons instead of one, and this poses a problem because over-reduced benzyl viologen is colorless and precipitates.

In this way, zinc pellets were used to (pre-)reduce the mediator before it was added to the reaction mixture. Firstly, the reduction of the mediator by zinc was optimized: the optimum time the zinc had to be in contact with the mediator, and the concentration of mediator necessary to achieve a stable and adequate level of reduced mediator were determined. This was achieved by monitoring the chemical oxidation of the mediator after its addition to the reaction mixture. Results showed the ideal incubation time was between 12 and 16h for methyl viologen, and about 13h if benzyl viologen was used instead. In either case, a mediator concentration of 12.5 mM yielded the most stable results.

Although the employment of the zinc pellet method to reduce the mediator allowed for a good replicate quality it also introduced variability in the assay due to difficulties in adding the same ratio of reduced and oxidized mediator molecules in each

experiment, making it difficult to achieve consistent results. An added challenge of performing these assays derives from the necessity of keeping the mediators reduced. As the standard reduction potentials for methyl and benzyl viologen are -450 and -350 mV v*ersus* NHE, respectively, even the smallest concentration of oxygen in the reaction mixture can oxidize them immediately [81]. Thus, although the lower standard reduction potential of methyl viologen would thermodynamically favor the carbon dioxide reduction reaction (E^0 = -420 mV) it was decided to employ benzyl viologen as a mediator in these assays. In addition, after studying the molar extinction coefficient for both viologens at different pHs, it was determined that reduced benzyl viologen was more stable than methyl viologen in the range between pH 6 and 8.

The kinetic assays for CO_2 reduction, presented in Figure III.16 show this reaction, catalyzed by *Dd* Fdh, in the presence of benzyl viologen displayed a Michaelis-Menten behavior.

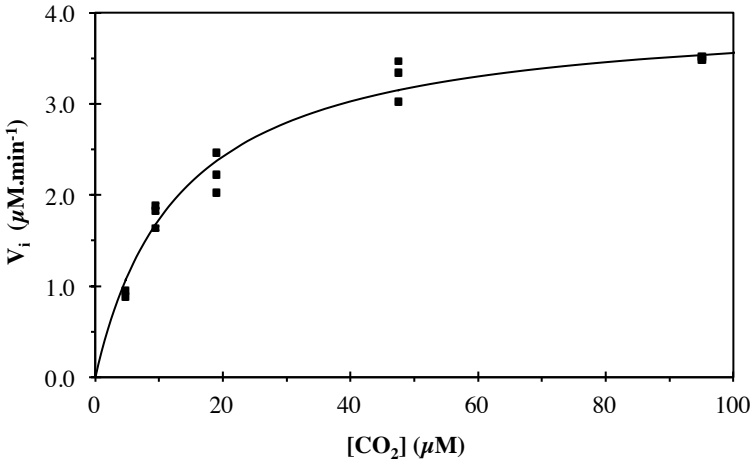

Figure III.16 – Kinetics of carbon dioxide reduction catalyzed by *D. desulfuricans* ATCC 27774 Fdh (■). The initial rates of carbon dioxide reduction were measured by monitoring the oxidation of the mediator, benzyl viologen, in 100 mM phosphate buffer pH 6.8 catalyzed by 15 nM Fdh. **Line:** fitting of the experimental data to a Michaelis-Menten equation with kinetic parameters K_M = 13.3 µM and V_{max} = 4 µM.min^{-1}.

Table III-8 resumes the preliminary kinetic parameters determined for carbon dioxide reduction, catalyzed by Fdh in the presence of benzyl viologen obtained by least square fit to the Michaelis-Menten equation, together with the kinetic parameters determined for formate dehydrogenases isolated from other organisms.

Table III-8 – Kinetic parameters for carbon dioxide reduction catalyzed by formate dehydrogenases isolated from diverse organisms.

	k_{cat} (s^{-1})	K_M (μM)	k_{cat}/K_M	Reference
Mo-Fdh *D. desulfuricans* ATCC 27774*	4.6 ± 0.2	13 ± 1	0.24	This work
W-Fdh *Syntrophobacter fumaroxidans* Fdh 1†	5250	ND	-	[72]
W-Fdh *Syntrophobacter fumaroxidans* Fdh 2†	183	ND	-	[72]
NADH-W-Fdh *Clostridium carboxidivorans*¶	0.08	ND	-	[80]
NADH-Mo-Fdh *Rhodobacter capsulatus*¶	1.48	ND	-	[79]

Mediators employed: * - benzyl viologen; † - methyl viologen; ¶ - NADH.

ND, not determined.

The k_{cat} values, presented in Table III-8, for carbon dioxide reduction by *Syntrophobacter fumaroxidans* Fdh 1 is nearly thirty times higher than that of Fdh 2. This suggests that Fdh 1 might be involved in metabolic pathways that led to carbon dioxide reduction while Fdh 2 must be linked to those involved in formate oxidation. With the exception of Fdh 1 from *Syntrophobacter fumaroxidans* all other formate dehydrogenases have a lower k_{cat} for the carbon dioxide reduction, when compared to that obtained for formate oxidation (Table III-7). After comparing the kinetic parameters for both reactions it is possible to assert that *Dd* Fdh is roughly nine times less efficient performing the reduction of carbon dioxide and that this reaction exhibits a turnover constant about thirty times slower. Even if we consider that only half of the enzyme used in the assays was active, the turnover constant is still one order of magnitude lower than for the formate oxidation reaction.

With the limited data available, it can be suggested that there is a clear division between dependent- and independent-NADH Fdhs, regardless of the metal that comprises their active site, with NADH-dependent Fdhs exhibiting a lower turnover constant. Although these results also reinforce the supposition that the enzyme as a whole, rather than the metal in the active site is responsible for the k_{cat}, for NADH-independent enzymes there is apparently a trend in which W-Fdhs have a higher turnover constant which is in line with the general accepted premise that only W-Fdhs are able to catalyze carbon dioxide reduction. This premise rises from the fact that the lower reduction potential of tungsten turns tungsten active sites into better reducing agents, when compared to molybdenum active sites that are considered better oxidant

agents [82,83]. Some authors also suggest that the properties of the metal center can be modulated through differences in the pyranopterin cofactor [82,84]. These differences may involve the extensive hydrogen bonding interactions between the pyranopterin cofactor and the protein matrix, that could facilitate electron transfer to (or from) the metal center [85]. Nonetheless, since only a small number enzymes have been characterized and kinetic parameters determined for the catalysis of both reactions, formate oxidation and carbon dioxide reduction, it is still early to make generalizations in regard to the catalytic efficiency of these enzymes and its relation to the metal in their active-site.

IV. CONCLUSIONS, FINAL REMARKS AND FUTURE WORK

IV. CONCLUSIONS, FINAL REMARKS AND FUTURE WORK

Carbon dioxide is a greenhouse effect gas, mainly produced by man-made activities such as the burning of fossil-fuels. This is leading to an increase in its atmospheric concentration, which in turn has the potential to change climate patterns. As carbon dioxide is a stable and unreactive molecule it is difficult to employ it in the synthesis of other compounds. Furthermore, the only large-scale process known to remove it from the atmosphere and employ it in the synthesis of energy carrying compounds is photosynthesis. No industrial process currently exists to sequester carbon dioxide and for its subsequent transformation into useful fuels or chemicals.

The purpose of this work was to explore formate dehydrogenases as biocatalysts for carbon dioxide reduction into formate. Formate is one of the simplest hydrocarbons; it is already used industrially as a building block for more complex molecules and research is making way for its employment in the development of safer fuel cells. The carbon dioxide reduction reaction is not new, as W-Fdhs have been reported to catalyze it. The novelty in this work is that, for the first time, we characterized this reaction for a NAD^+-independent Mo-Fdh.

To do this characterization large amounts of purified enzyme were needed. So, from a selected range of media, it was determined which ones allowed the recovery of a greater cellular mass. Having established that VMN, ATCC 1249 and ATCC 2755 media fulfilled this condition we endeavored efforts to determine of these, what was the one that provided growth conditions to increase Fdh expression. After in gel activity assays, to evaluate Fdh activity, VMN was the medium chosen to perform subsequent cell growths. Next, assays were done that suggested the cells should be harvested at the stationary growth stage, as in this phase they presented a higher Fdh expression level.

Before performing kinetic assays to characterize the formate oxidation reaction it was necessary to optimize the reaction conditions. Preliminary Fdh reduction studies were done to better understand the redox processes that occur throughout the steady-state kinetic assays. Although the reduced spectra exhibited the typical

characteristics of a heme-*c* spectrum, with Soret, α and β bands, at 419, 523 and 552 nm, respectively. It is still possible to observe, at 400 nm, the reduction of the [4Fe-4S] cluster. These assays also revealed that the addition of a sulfhydryl reducing agent only partially reduces the hemes, and that only the addition of formate has the ability to completely reduce them. These experiments also helped to define how the kinetic assays would be performed, as the incubation of the enzyme with formate prior to the start of the kinetic assays is necessary to activate the enzyme to yield its maximum activity. Being so, for the kinetic assays the reaction was triggered with the addition of mediator instead of being triggered with the addition of substrate.

This work made it possible to demonstrate that a Mo-Fdh is also able to catalyze the carbon dioxide reduction reaction, and to determine the kinetic parameters for the formate oxidation and carbon dioxide reduction reactions, summarized in Table IV-1.

Table IV-1 – Kinetic parameters for formate oxidation and carbon dioxide reduction in the presence of benzyl viologen by *D. desulfuricans* Fdh.

D. desulfuricans ATCC 27774 Fdh	k_{cat} (s^{-1})	K_M (μM)	k_{cat}/K_M
Formate oxidation reaction	146 ± 2	49 ± 2	2.97
Carbon dioxide reduction reaction	4.6 ± 0.2	13 ± 1	0.34

Despite the advances accomplished in recent years, there is still a myriad of questions unanswered in regard to carbon dioxide reduction catalyzed by Fdhs namely: how are the catalytic mechanisms for formate oxidation and carbon dioxide reduction? Within Fdhs what features allow some to be better catalysts? And can we employ them in bioremediation processes?

To answer these questions, upcoming studies will need to focus in the characterization of these enzymes, before aiming to understand if and how we can take advantage of them as bioremediation agents. For such characterization it is necessary to venture in the development of growth conditions that favor Fdh expression. Such experiments may lead to the employment of different carbon sources, such as pyruvate and acetate, in the growth media, allowing to understand how its use influences the expression of Fdh. The kinetic characterization would benefit if a more stable mediator was employed, as viologens, due to their highly negative standard reduction potential

are, in their reduced form, very unstable under an aerobic atmosphere. However, as the carbon dioxide reduction reaction requires a reduction potential of at least -420 mV, as far as we know, viologens are the only mediators with sufficient potential to allow its characterization. Nonetheless, the reproducibility of the assays can be further increased with the development of a more efficient way to eliminate oxygen from the assays and with improvements to the experimental technique employed to reduce the mediator. These improvements would allow it to become more stable and might prevent its precipitation approximately 8 hours after preparation as it currently happens. Effort should also go in to the development of a way to consistently achieve the same ratio of reduced mediator, as its reduction potential is affected by the reduced/oxidized ratio of molecules [86]. Future studies should also characterize the kinetic parameters of the carbon dioxide reduction reaction for *Dd* but also be extended to other Mo/W-Fdhs as these studies might enable us to infer about the influence the metal cofactor has on the kinetic parameters of the reaction. The long-term objectives are to increase the stability of the enzymatic system, in particular its susceptibility to oxygen that precludes its use in biotechnological applications. Being the ultimate goal to use this enzymatic system as a model to develop a new, faster, cheaper and specific synthetic catalyst for future application in the capture and valorization of carbon dioxide.

V. BIBLIOGRAPHY

V. BIBLIOGRAPHY

1 Hoeven, M. (2012) CO_2 emissions from fuel combustion, pp 1–51, Paris.

2 Tans, P. and Keeling, R. (2014) Trends in Atmospheric Carbon Dioxide.

3 Schneider, J. and Fujita, E. (2013) Carbon Dioxide Capture and Activation. Compr. Inorg. Chem. II (Reedijk, J., and Poeppelmeier, K., eds.) Second Edi., pp 475–504, Elsevier, Oxford.

4 Halmann, M. and Steinberg, M. (1999) Greenhouse Gas Carbon Dioxide Mitigation: Science and Technology 1st Edi., pp 1–568, CRC Press, Boca Raton, Florida.

5 Hu, B., Guild, C. and Suib, S. L. (2013) Thermal, electrochemical, and photochemical conversion of CO_2 to fuels and value-added products. J. CO_2 Util. **1**, 18–27.

6 Hoeven, M. (2013) CO_2 emissions from fuel combustion highlights 2013, Paris.

7 Arakawa, H., Aresta, M., Armor, J. N., Barteau, M. A., Beckman, E. J., Bell, A. T., Bercaw, J. E., Creutz, C., Dinjus, E., Dixon, D. A., et al. (2001) Catalysis Research of Relevance to Carbon Management: Progress, Challenges, and Opportunities. Chem. Rev. **101**, 953–996.

8 Orr, Jr., F. M. (2009) CO_2 capture and storage: are we ready? Energy Environ. Sci. **2**, 449–458.

9 Aresta, M. and Dibenedetto, A. (2007) Utilisation of CO_2 as a chemical feedstock: opportunities and challenges. Dalton Trans. 2975–2992.

10 Medvecky, F., Lacey, J. and Ashworth, P. (2013) Examining the Role of Carbon Capture and Storage Through an Ethical Lens. Sci. Eng. Ethics Epub ahead of print.

11 Reda, T., Plugge, C. M., Abram, N. J. and Hirst, J. (2008) Reversible interconversion of carbon dioxide and formate by an electroactive enzyme. Proc. Natl. Acad. Sci. U. S. A. **105**, 10654–10658.

12 Singh, A., Pant, D., Olsen, S. I. and Nigam, P. S. (2012) Key issues to consider in microalgae based biodiesel production. Energy Educ. Sci. Technol. Part A Energy Sci. Res. **29**, 687–700.

13 Alvarez-Guerra, M., Quintanilla, S. and Irabien, A. (2012) Conversion of carbon dioxide into formate using a continuous electrochemical reduction process in a lead cathode. Chem. Eng. J. **207-208**, 278–284.

14 Kang, P., Meyer, T. J. and Brookhart, M. (2013) Selective electrocatalytic reduction of carbon dioxide to formate by a water-soluble iridium pincer catalyst. Chem. Sci. **4**, 3497–3502.

15 Jessop, P. G., Takao, I. and Noyori, R. (1994) Homogeneous catalytic hydrogenation of supercritical carbon dioxide. Nature **368**, 231–233.

16 Yotsuhashi, S., Hashiba, H., Deguchi, M., Zenatani, Y. and Hinogami, R. (2012) Highly efficient photochemical HCOOH production from CO_2 and water using an inorganic system. AIP Adv. **2**.

17 Sato, S., Arai, T., Morikawa, T., Uemura, K., Suzuki, T. M., Tanaka, H. and Kajino, T. (2011) Selective CO_2 Conversion to Formate Conjugated with H_2O Oxidation Utilizing Semiconductor/Complex Hybrid Photocatalysts 15240–15243.

18 Desloover, J., Arends, J. B. a, Hennebel, T. and Rabaey, K. (2012) Operational and technical considerations for microbial electrosynthesis. Biochem. Soc. Trans. **40**, 1233–1238.

19 Bell, A. T. (2008) Basic Research Needs: Catalysis for Energy.

20 Alissandratos, A., Kim, H. and Easton, C. J. (2014) Formate production through carbon dioxide hydrogenation with recombinant whole cell biocatalysts. Bioresour. Technol. **164**, 7–11.

21 Erb, T. J. (2011) Carboxylases in natural and synthetic microbial pathways. Appl. Environ. Microbiol. **77**, 8466–8477.

22 Fuchs, G. (2011) Alternative pathways of carbon dioxide fixation: insights into the early evolution of life? Annu. Rev. Microbiol., pp 631–658.

23 Bassham, J. A., Benson, A. A. and Calvin, M. (1950) The path of carbon in photosynthesis: VIII. The rôle of malic acid. J. Biol. Chem. 781–787.

24 Thauer, R. K. (1998) Biochemistry of methanogenesis : a tribute to Marjory Stephenson. Microbiology **144**, 2377–2406.

25 Appel, A. M., Bercaw, J. E., Bocarsly, A. B., Dobbek, H., DuBois, D. L., Dupuis, M., Ferry, J. G., Fujita, E., Hille, R., Kenis, P. J. A., et al. (2013) Frontiers, Opportunities, and Challenges in Biochemical and Chemical Catalysis of CO_2 Fixation. Chem. Rev. **113**, 6621–6658.

26 Hummel, W. (1997) New Alcohol Dehydrogenases for the Synthesis of Chiral Compounds. Adv. Biochem. Eng. Biotechnol. **58**, 147–184.

27 Kragl, U., Kruse, W., Humme, W. and Wandref, C. (1996) Enzyme Engineering Aspects of Biocatalysis: Cofactor Regeneration as Example. Biotechnol. Bioeng. **52**, 309–319.

28 Popov, V. O. and Tishkov, V. I. (2003) NAD^+-dependent formate dehydrogenase. From a model enzyme to a versatile biocatalyst. Res. Signpost, pp 345–369, Moscow.

29 Tishkov, V. I. and Popov, V. O. (2004) Catalytic Mechanism and Application of Formate Dehydrogenase. Biochem. **69**, 1252–1267.

30 Popov, V. O. and Lamzin, V. S. (1994) NAD^+-dependent formate dehydrogenase. Biochem. J. **301**, 625–643.

31 Unden, G. and Bongaerts, J. (1997) Alternative respiratory pathways of Escherichia coli : energetics and transcriptional regulation in response to electron acceptors. Biochim. Biophys. Acta **1320**, 217–234.

32 Richardson, D. J. (2000) Bacterial respiration : a flexible process for a changing environment. Microbiology **146**, 551–571.

33 Da Silva, S. M., Pimentel, C., Valente, F. M. a, Rodrigues-Pousada, C. and Pereira, I. a C. (2011) Tungsten and molybdenum regulation of formate dehydrogenase expression in Desulfovibrio vulgaris Hildenborough. J. Bacteriol. **193**, 2909–2916.

34 Ihara, M., Kawano, Y., Urano, M. and Okabe, A. (2013) Light Driven CO_2 Fixation by Using Cyanobacterial Photosystem I and NADPH-Dependent Formate Dehydrogenase. PLoS One **8**, 1–8.

35 Hornsey, D. J. (1971) An investigation of formate metabolism in bacteria using radiorespirometry. Int. J. Appl. Radiat. Isot. **22**, 381–382.

36 Leonhartsberger, S., Korsa, I. and Böck, A. (2002) The molecular biology of formate metabolism in enterobacteria. J. Mol. Microbiol. Biotechnol. **4**, 269–276.

37 Jormakka, M., Byrne, B. and Iwata, S. (2003) Formate dehydrogenase - A versatile enzyme in changing environments. Curr. Opin. Struct. Biol. **13**, 418–423.

38 Crable, B. R., Plugge, C. M., McInerney, M. J. and Stams, A. J. M. (2011) Formate formation and formate conversion in biological fuels production. Enzyme Res. **2011**, 1–8.

39 Gonzalez, P. J., Rivas, M. G., Mota, C. S., Brondino, C. D., Moura, I. and Moura, J. J. G. (2013) Periplasmic nitrate reductases and formate dehydrogenases: Biological control of the chemical properties of Mo and W for fine tuning of reactivity, substrate specificity and metabolic role. Coord. Chem. Rev. **257**, 315–331.

40 Romão, M. J. (2009) Molybdenum and tungsten enzymes: a crystallographic and mechanistic overview. Dalt. Trans. 4053–4068.

41 Magalon, A., Fedor, J. G., Walburger, A. and Weiner, J. H. (2011) Molybdenum enzymes in bacteria and their maturation. Coord. Chem. Rev. **255**, 1159–1178.

42 Hille, R. (2013) The molybdenum oxotransferases and related enzymes. Dalt. Trans. **42**, 3029–3042.

43 Hille, R. (1996) The Mononuclear Molybdenum Enzymes. Chem. Rev. **96**, 2757–2816.

44 Brondino, C. D., Rivas, M. G., Romão, M. J., Moura, J. J. G. and Moura, I. (2006) Structural and electron paramagnetic resonance (EPR) studies of mononuclear molybdenum enzymes from sulfate-reducing bacteria. Acc. Chem. Res. **39**, 788–796.

45 Yu, S., Zhu, L., Zhou, C., An, T., Zhang, T., Jiang, B. and Mu, W. (2014) Promising properties of a formate dehydrogenase from a methanol-assimilating yeast Ogataea parapolymorpha DL-1 in His-tagged form. Appl. Microbiol. Biotechnol. **98**, 1621–1630.

46 Ferry, J. G. (1990) Formate dehydrogenase. FEMS Microbiol. Rev. **7**, 377–382.

47 Bommarius, A. S., Schwarm, M., Stingl, K., Kottenhahn, M., Huthmacher, K. and Drauz, K. (1995) Synthesis and Use of Enantiomerically Pure tert-Leucine. Tetrahedron: Asymmetry **6**, 2851–2888.

48 Tishkov, V. I. and Popov, V. O. (2006) Protein engineering of formate dehydrogenase. Biomol. Eng. **23**, 89–110.

49 Jayabalan, R., Sathishkumar, M., Jeong, E. S., Mun, S. P. and Yun, S. E. (2012) Immobilization of flavin adenine dinucleotide (FAD) onto carbon cloth and its application as working electrode in an electroenzymatic bioreactor. Bioresour. Technol. **123**, 686–689.

50 Rivas, M. G., González, P. J., Brondino, C. D., Moura, J. J. G. and Moura, I. (2007) EPR characterization of the molybdenum(V) forms of formate dehydrogenase from Desulfovibrio desulfuricans ATCC 27774 upon formate reduction. J. Inorg. Biochem. **101**, 1617–1622.

51 Berg, I. A. (2011) Ecological Aspects of the Distribution of Different Autotrophic CO_2 Fixation Pathways. Appl. Environ. Microbiol. **77**, 1925–1936.

52 Nguyen, N. T., Yatabe, T., Yoon, K. and Ogo, S. (2014) Molybdenum-containing membrane-bound formate dehydrogenase isolated from Citrobacter sp. S-77 having high stability against oxygen, pH, and temperature. J. Biosci. Bioeng., 1–6.

53 Yoshimoto, M., Kunihiro, N., Tsubomura, N. and Nakayama, M. (2013) Preparation of liposome-coupled NADH and evaluation of its affinity toward formate dehydrogenase based on deactivation kinetics of the enzyme. Colloids Surfaces B Biointerfaces. **109**, 40–44.

54 Gronenberg, L. S., Marcheschi, R. J. and Liao, J. C. (2013) Next generation biofuel engineering in prokaryotes. Curr. Opin. Chem. Biol. **17**, 462–471.

55 Miyatani, R. and Amao, Y. (2004) Photochemical synthesis of formic acid from CO_2 with formate dehydrogenase and water-soluble zinc porphyrin. J. Mol. Catal. B Enzym. **27**, 121–125.

56 Nicolaou, S. A., Gaida, S. M. and Papoutsakis, E. T. (2010) A comparative view of metabolite and substrate stress and tolerance in microbial bioprocessing : From biofuels and chemicals, to biocatalysis and bioremediation. Metab. Eng. **12**, 307–331.

57 Ketterer, L. and Keusgen, M. (2010) Amperometric sensor for cyanide utilizing cyanidase and formate dehydrogenase. Anal. Chim. Acta. **673**, 54–59.

58 Fröhlich, P., Albert, K. and Bertau, M. (2011) Formate dehydrogenase: A biocatalyst with novel applications in organic chemistry. Org. Biomol. Chem. **9**, 7941–7950.

59 Boyington, J. C. (1997) Crystal Structure of Formate Dehydrogenase H: Catalysis Involving Mo, Molybdopterin, Selenocysteine, and an Fe4S4 Cluster. Science (80-.). **275**, 1305–1308.

60 Raaijmakers, H. C. a and Romão, M. J. (2006) Formate-reduced E. coli formate dehydrogenase H: The reinterpretation of the crystal structure suggests a new reaction mechanism. J. Biol. Inorg. Chem. **11**, 849–54.

61 Moura, J. J. G., Brondino, C. D., Trincão, J. and Romão, M. J. (2004) Mo and W bis-MGD enzymes: Nitrate reductases and formate dehydrogenases. J. Biol. Inorg. Chem. **9**, 791–799.

62 Raaijmakers, H., Macieira, S., Dias, M., Teixeira, S., Bursakov, S., Huber, R., Moura, J. G., Moura, I. and Roma, M. J. (2002) Gene Sequence and the 1.8 A of the Tungsten-Containing Formate Dehydrogenase from Desulfovibrio gigas. Structure **10**, 1261–1272.

63 Raaijmakers, H., Teixeira, S., Dias, J. M., Almendra, M. J., Brondino, C. D., Moura, I., Moura, J. J. G. and Romão, M. J. (2001) Tungsten-containing formate dehydrogenase from Desulfovibrio gigas: Metal identification and preliminary structural data by multi-wavelength crystallography. J. Biol. Inorg. Chem. **6**, 398–404.

64 Almendra, M. J., Brondino, C. D., Gavel, O., Pereira, A. S., Tavares, P., Bursakov, S., Duarte, R., Caldeira, J., Moura, J. J. G. and Moura, I. (1999) Purification and characterization of a tungsten-containing formate dehydrogenase from Desulfovibrio gigas. Biochemistry **38**, 16366–16372.

65 Costa, C., Teixeira, M. and LeGall, J. (1997) Formate dehydrogenase from Desulfovibrio desulfuricans ATCC 27774: isolation and spectroscopic characterization of the active sites (heme, iron-sulfur centers and molybdenum). JBIC **2**, 198–208.

66 Mota, C. S., Rivas, M. G., Brondino, C. D., Moura, I., Moura, J. J. G., González, P. J. and Cerqueira, N. M. F. S. a. (2011) The mechanism of formate oxidation by metal-dependent formate dehydrogenases. J. Biol. Inorg. Chem. **16**, 1255–1268.

67 Leopoldini, M., Chiodo, S. G., Toscano, M. and Russo, N. (2008) Reaction mechanism of molybdoenzyme formate dehydrogenase. Chem. - A Eur. J. **14**, 8674–8681.

68 Hensgens, C. M. H., Hagen, W. R. and Hansen, T. A. (1995) Purification and Characterization of a Benzylviologen-Linked , Tungsten-Containing Aldehyde Oxidoreductase from Desulfovibrio gigas. J. Bacteriol. **177**, 6195–6200.

69 Kletzin, A. and Adams, M. W. W. (1996) Tungsten in biological systems. FEMS Microbiol. Rev. **18**, 5–63.

70 Walker, J. M. (2002) The Protein Protocols Handbook Second Edi., Humana Press, New Jersey.

71 Baranyi, J. and Roberts, T. A. (1994) A dynamic approach to predicting bacterial growth in food. Int. J. Food Microbiol. **23**, 277–294.

72 De Bok, F. a. M., Hagedoorn, P.-L., Silva, P. J., Hagen, W. R., Schiltz, E., Fritsche, K. and Stams, A. J. M. (2003) Two W-containing formate dehydrogenases (CO_2-reductases) involved in syntrophic propionate oxidation by Syntrophobacter fumaroxidans. Eur. J. Biochem. **270**, 2476–2485.

73 Silveira, C. Personal communication.

74 Mota, C. S., Valette, O., González, P. J., Brondino, C. D., Moura, J. J. G., Moura, I., Dolla, A. and Rivas, M. G. (2011) Effects of molybdate and tungstate on expression levels and biochemical characteristics of formate dehydrogenases

produced by Desulfovibrio alaskensis NCIMB 13491. J. Bacteriol. **193**, 2917–2923.

75 Lukesh, J. C., Palte, M. J. and Raines, R. T. (2012) A potent, versatile disulfide-reducing agent from aspartic acid. J. Am. Chem. Soc. **134**, 4057–4059.

76 Mayhew, S. G. (1978) The Redox Potential of Dithionite and SO_2^- from Equilibrium Reactions with Flavodoxins, Methyl Viologen and Hydrogen plus Hydrogenase. Eur. J. Biochem. **85**, 535–547.

77 Cerqueira, N. M. F. S. a, Fernandes, P. a., Gonzalez, P. J., Moura, J. J. G. and Ramos, M. J. (2013) The sulfur shift: An activation mechanism for periplasmic nitrate reductase and formate dehydrogenase. Inorg. Chem. **52**, 10766–10772.

78 Axley, M. J. and Grahame, D. A. (1991) Kinetics for formate dehydrogenase of Escherichia coli formate-hydrogenlyase. J. Biol. Chem. **266**, 13731–13736.

79 Hartmann, T. and Leimkühler, S. (2013) The oxygen-tolerant and NAD^+-dependent formate dehydrogenase from Rhodobacter capsulatus is able to catalyze the reduction of CO_2 to formate. FEBS J. **280**, 6083–6096.

80 Alissandratos, A., Kim, H.-K., Matthews, H., Hennessy, J. E., Philbrook, A. and Easton, C. J. (2013) Clostridium carboxidivorans strain P7T recombinant formate dehydrogenase catalyzes reduction of CO_2 to formate. Appl. Environ. Microbiol. **79**, 741–744.

81 Tsukahara, K. and Wilkins, R. G. (1985) Kinetics of Reduction of Eight Viologens by Dithionite Ion. J. Am. Chem. Soc. **107**, 2632–2635.

82 McNamara, J. P., Joule, J. a, Hillier, I. H. and Garner, C. D. (2005) Promotion of oxygen atom transfer in Mo and W enzymes by bicyclic forms of the pterin cofactor. Chem. Commun. (Camb). 177–179.

83 Sugimoto, H. and Tsukube, H. (2008) Chemical analogues relevant to molybdenum and tungsten enzyme reaction centres toward structural dynamics and reaction diversity. Chem. Soc. Rev. **37**, 2609–2619.

84 McNamara, J. P., Hillier, I. H., Bhachu, T. S. and Garner, C. D. (2005) The nature and function of the catalytic centres of the DMSO reductases. Dalton Trans. 3572–3579.

85 Enemark, J. H. and Garner, C. D. (1997) The coordination chemistry and function of the molybdenum centres of the oxomolybdoenzymes. J. Biol. Inorg. Chem. **2**, 817–822.

86 Michaelis, B. Y. L. and Hill, E. S. (1933) The viologen indicators. J. Gen. Physiol. 859–873.

87 Unstained Protein Molecular Weight Marker. (n.d.). Retrieved July 8, 2014, from http://www.thermoscientificbio.com/protein-electrophoresis/unstained-protein-molecular-weight-marker/.

VI. APPENDIXES

VI. APPENDIXES

VI.1. Growth Media

The following tables contain the formulae to prepare each of the media used throughout this work. Unless otherwise stated, quantities given relate to one liter of medium or supplement.

Table VI-1 – ATCC Medium: 42 *Desulfovibrio* medium.

Composition	
$Mg(SO_4)$	1.5 g
Na_2SO_4	2 g
$Fe(NH_4)_2(SO_4)_2.6H_2O$	0.1 g
Glucose	5 g
Peptone	5 g
Beef Extract	3 g
Yeast Extract	0.2 g

Table VI-2 – ATCC Medium: 1249 Modified Baar's medium for sulfate reducers.

Component I	
$Mg(SO_4)$	2 g
Sodium Citrate	5 g
$CaSO_4$	1 g
NH_4Cl	1 g
H_2O	400 mL

Component II	
K_2HPO_4	0.5 g
H_2O	200 mL

Component III	
Sodium Lactate	3.5 g
Y	1.0 g
H_2O	400 mL

Adjust the pH of each component to pH 7.5 and autoclave. Mix the three components aseptically and tube under 100% Ar while warm to exclude as much oxygen as possible.

Component IV	
$Fe(NH_4)_2(SO_4)_2$	5% w/v

Filter-sterilize 5% $Fe(NH_4)_2(SO_4)_2$, and add 0.1 mL to 5.0 mL of medium prior to inoculation.

Table VI-3 – ATCC Medium: 2755 *Desulfovibrio* medium.

Solution A	
K_2HPO_4	0.5 g
NH_4Cl	1 g
Na_2SO_4	1 g
$CaCl_2.2H_2O$	0.1 g
$MgSO_4.7H_2O$	2 g
Sodium Lactate	2 g
Yeast Extract	1 g
Resazurin	1 mg
H_2O	980 mL

Solution B	
$FeSO_4.7H_2O$	0.5 g
H_2O	10 mL

Solution C	
Na-thioglycolate	0.1 g
Ascorbic Acid	0.1 g
H_2O	10 mL

Dissolve the ingredients of each solution in the appropriate quantities of water. Bring solution A to boil for a few minutes. Autoclave solution A at 121°C and cool to room temperature while gassing with oxygen-free N_2 gas.

Filter sterilize solutions B and C. Add both filtered solutions to solution A and continue to gas the complete media. Adjust to pH 7.8 with NaOH, and distribute under N_2 in anaerobic tubes. During distribution continuously swirl the medium to keep the grey precipitate suspended.

Table VI-4 – ATCC Medium: 27774 *Desulfovibrio desulfuricans* medium.

Composition	
K_2HPO_4	0.5 g
$NaNO_3$	2.5 g
$Mg(NO_3)_2.6H_2O$	0.73 g
$Na_2S.9H_2O$	0.5 g
$CaCl_2.2H_2O$	0.2 g
$FeCl_2.4H_2O$	3.55 g
Sodium Lactate	12.5 mL
Yeast Extract	1 g
Cys.HCl	0.5 g
Resazurin*	1.0 mL

* - Resazurin solution 0.1% (w/v)

Adjust to pH 7.0.

Table VI-5 – *Desulfovibrio desulfuricans* medium LSYC.

Composition	
K_2HPO_4	0.5 g
NH_4Cl	1 g
Na_2SO_4	2 g
$CaCl_2.2H_2O$	0.1 g
$Fe(NH_4)_2(SO_4)_2.6H_2O$	0.1 g
Sodium Lactate	3.5 g
Yeast Extract	1 g
Cys.HCl	1 g

Adjust to pH 7.0.

Table VI-6 – VMN medium.

Composition		
KH_2PO_4	0.5 g	
$NaNO_3$	2.4 g	
NH_4Cl	1.0 g	
$MgCl.6H_2O$	0.05 g	
$CaCl_2.2H_2O$	0.04 g	
Sodium Lactate	6.0 g	
Sodium Citrate	0.3 g	
$FeCl.4H_2O$	0.003 g	
NZCYM Broth	2.0 g	
Triptone	2.0 g	
Vitamin Solution	2 mL	(Table VI-7)
Wolfes Elixir	1 mL	(Table VI-8)

Adjust for pH 7.5 +/- 0.05. The vitamin solution is filter sterilized and added after the medium has been sterilized.

Table VI-7 – Vitamin Solution for VMN medium, final volume 200 mL.

Composition	
Riboflavin	0.02 g
Raise the pH with NaOH to improve solubility. Adjust to pH 7.4 with Tris-HCl 50 mM.	
Niacin	0.05 g
Thiamine	0.06 g
Pantothenic acid	0.06 g
Pyridoxine	0.06 g
Cyanocobalamin	0.005 g
Sodium ascorbate	0.2 g
Biotin	0.001 g

Keep frozen and in the dark. Must be filter sterilized before use.

Table VI-8 – Wolfes Elixir for VMN medium.

Composition	
Nitriloacetic acid	1.5 g
Adjust pH to 6.5 with KOH (5M)	
$MgSO_4.7H_2O$	3.0 g
$MnSO_4.4.H_2O$	0.5 g
NaCl	1.0 g
$FeSO_4.7H_2O$	0.1 g
$CoSO_4.7H_2O$	0.1 g
$NiCl_2.6H_2O$	0.1 g
$CuCl_2.2H_2O$	0.1 g
$ZnSO_4.7H_2O$	0.1 g
$CuSO_4.5H_2O$	0.01 g
$AlK(SO_4).12H_2O$	0.01 g
H_3BO_3	0.01 g
$Na_2MoO_4.2H_2O$	0.01 g
$Na_2SeO_3.5H_2O$	0.001 g

Table VI-9 – M medium.

Composition	
K_2HPO_4	0.47 g
NH_4Cl	1.9 g
$NaNO_3$	2.28 g
$MgCl_2.\ 6H_2O$	1.55 g
Sodium Lactate	10 mL
Yeast Extract	0.95 g

Adjust pH to 7.5. Autoclave medium for 20 minutes at 121ºC.

Table VI-10 – M medium, supplements.

Composition	
Oligo-elements “Fauque”	10 mL (Table VI-11)
$FeCl_2.4H_2O$	0.67 g/l Oligo
$CaCl_2.2H_2O$ 1M	1.3 mL
$Na_2S.3H_2O$	10 mL (1% w/v)

Supplements are added to the medium in anaerobic conditions, after it has been autoclaved.

Table VI-11 – Oligo-elements "Fauque".

Composition	
Nitriloacetic acid	12.8 g
Adjust pH to 6.5 with KOH (5M)	
$FeCl_2.4H_2O$	0.21 g
$MnCl_2.4H_2O$	0.1 g
$CoCl_2.6H_2O$	0.17 g
$ZnCl_2$	0.1 g
$CuCl_2.H_2O$	0.02 g
H_3BO_3	0.01 g
$Na_2MoO_4.2H_2O$	0.01 g
$Na_2SeO_3.5H_2O$	0.017 g
$NiCl_2.6H_2O$	0.128 g

VI.2. Gel electrophoresis

Polyacrylamide gel electrophoresis was employed throughout this work in native conditions (PAGE) to assess Fdh activity or in denaturant conditions (SDS-PAGE) to assess the purity of the collected fractions during the purification process. In either case the gels prepared had 7.5% (w/v) polyacrylamide and were prepared as showed in Table VI-12.

Table VI-12 – Preparation of a 7.5% polyacrylamide gel.

Stock Solutions	Concentration Gel (mL)	Running Gel (mL)
Solution I	-	0.75
Solution II	0.9	-
Solution III	0.3	1.67
H_2O	0.94	2.85
SDS 10% (μL)*	18	50
PSA 10% (w/v) (μL)	13.5	38
TEMED (μL)	2	2.5

* - SDS is employed only in SDS-PAGE. For PAGE, SDS is substituted by water.

Table VI-13 – Composition of the solutions employed.

Solution	Composition
I	Tris-HCl 1.5 M pH 8.8
II	Tris-HCl 1 M pH 6.8
III	Acrylamide/Bis Solution, 37.5:1

All samples were loaded into the gel with a sample buffer solution whose components are summarized in Table VI-14.

Table VI-14 – Composition of the sample buffer solution.

	Concentration
Tris-HCl pH 6.8	125 mM
SDS *	4%
β-mercaptoethanol*	5% (w/v)
Glycerol	10% (v/v)
Bromophenol Blue	0.02% (w/v)

* - SDS and β-mercaptoethanol are employed only in SDS-PAGE. For PAGE, β-mercaptoethanol and SDS are omitted.

All samples for SDS-PAGE were boiled for 2 minutes. All gels were run at a constant current of 40 mA per gel in Tris-Glycine buffer with the following composition:

Table VI-15 – Tris-Glycine buffer composition.

	Concentration
Tris-HCl pH 8.3	25 mM
Glycine	192 mM
SDS *	0.1%

* - SDS is employed only for SDS-PAGE. For PAGE, SDS is substituted by water.

All electrophoresis were done with a Mini-Protean Tetra System (Bio-Rad) using 8.3 x 7.3 cm handcast gels. The molecular weight marker used for the SDS-PAGE was Fermentas unstained protein molecular weight marker (Fermentas), consisting in a mixture of seven native proteins (14.4 to 116 kDa). A electrophoretic profile of the marker is depicted in Figure VI-1.

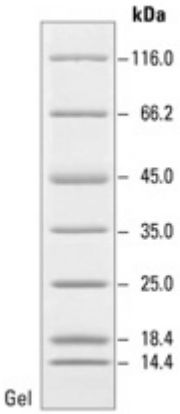

Figure VI.1 – Electrophoretic profile of Fermentas unstained protein marker in a 12% Tris-glycine gel (SDS-PAGE) [87]**.**

The gels were stained by immersion on a Coomassie blue solution and the excess dye was removed by immersion on a distaining solution. The composition of each of these solutions is presented below.

Table VI-16 – Coomassie blue dye solution.

	Concentration
Coomassie blue R250	0.25%
Methanol	50%
Acetic Acid	10%

Table VI-17 – Distaining solution.

	Concentration
Methanol	40%
Acetic Acid	10%

VI.3. Periplasmatic soluble extract preparation flowchart

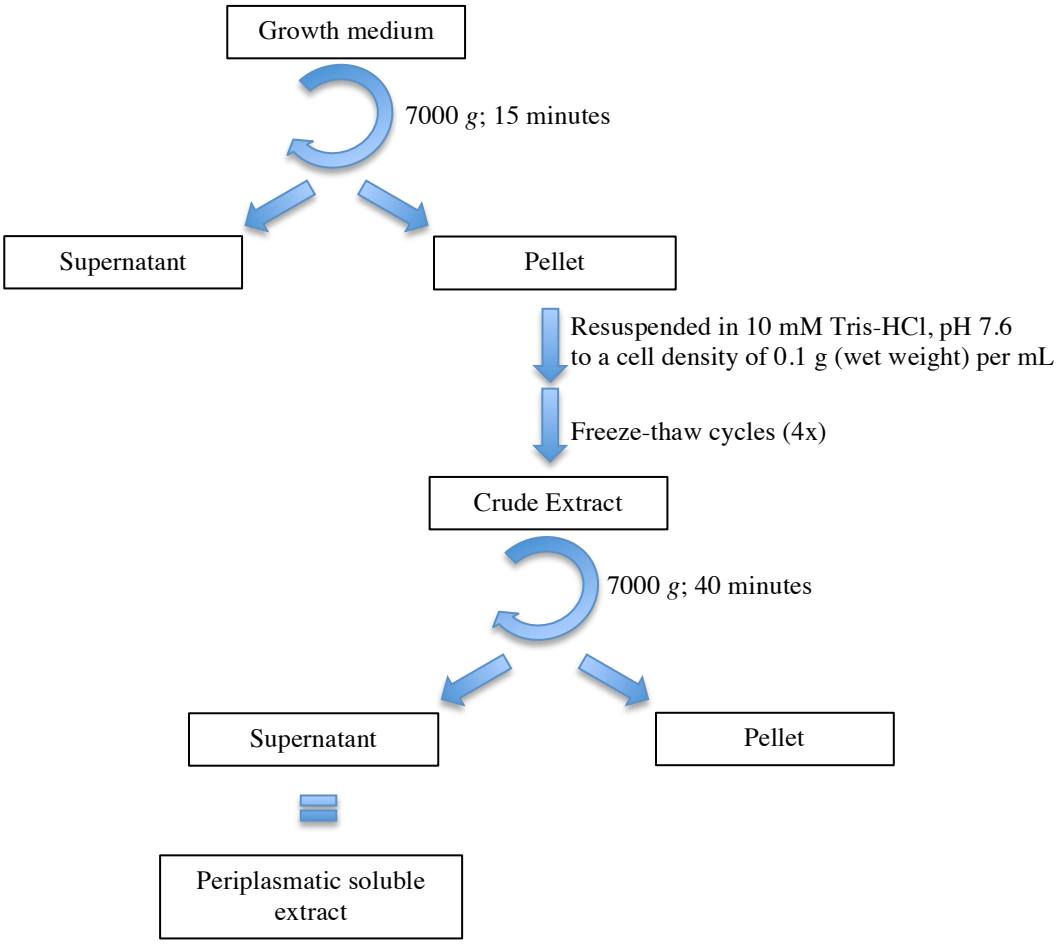

Figure VI.2 – Periplasmatic soluble extract preparation flowchart.

VI.4. Cell soluble extract preparation flowchart

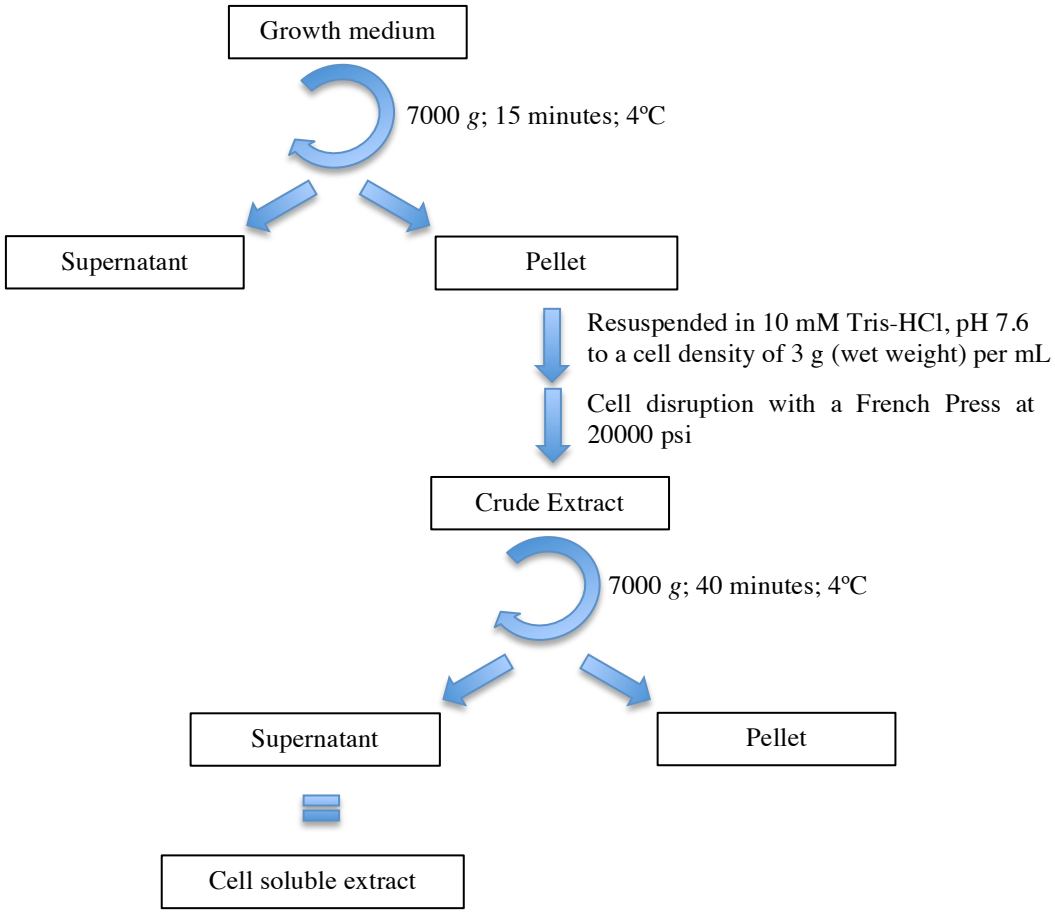

Figure VI.3 – Cell soluble extract preparation flowchart.

VI.5. Purification flowchart

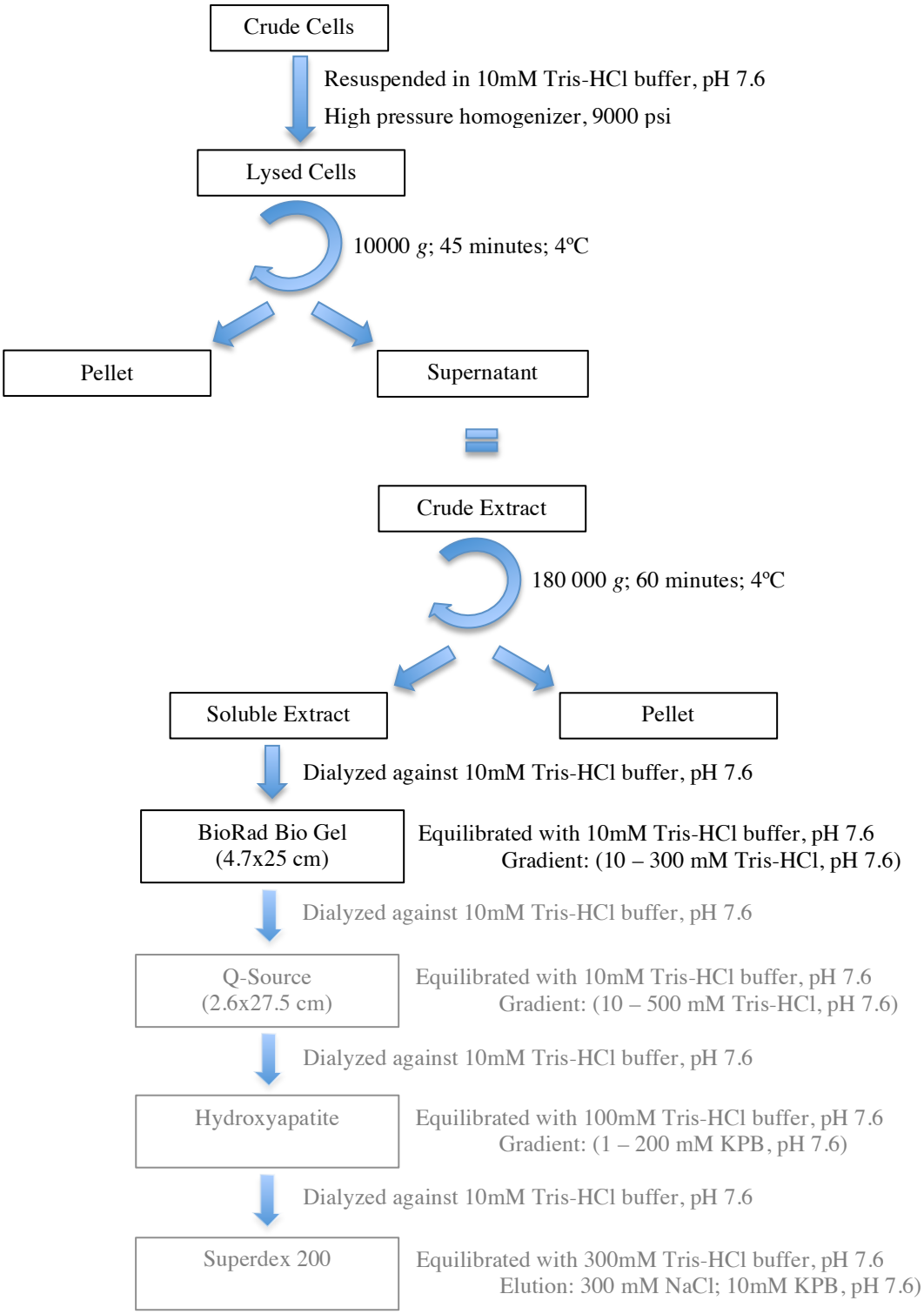

Figure VI.4 – *D. desulfuricans* ATCC 27774 purification flowchart. Procedures in grey were not done.

VI.6. Carbonate species and pH dependency

Figure VI.5 shows a representation of carbonate species and their dependency with pH.

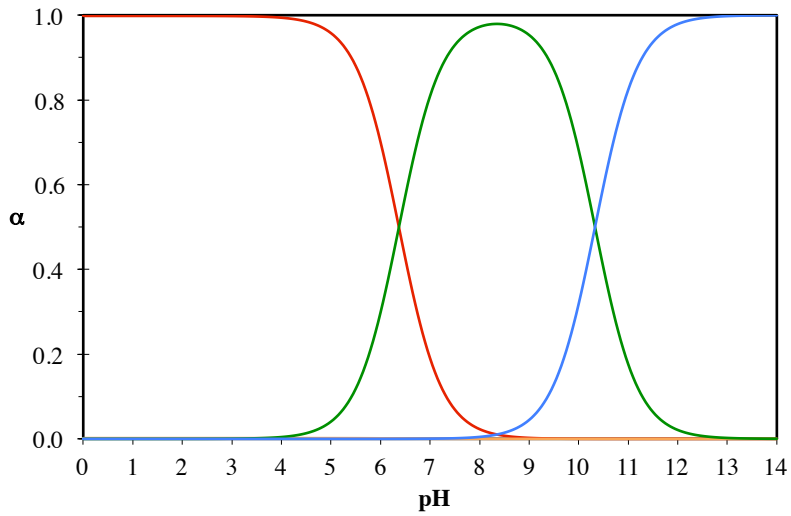

Figure VI.5 – Carbonate species present in solution and their dependency with the pH value. — CO_2; — H_2CO_3; — $(HCO_3)^-$; — $(CO_3)^{-2}$.

The equilibrium equations and constants employed to arrive at these results are presented in Eq. VII.1, Eq. VII.2 and Eq. VII.3.

(equation VII.1)

$$CO_2 + H_2O \overset{K_C}{\Leftrightarrow} H_2CO_3$$

(equation VII.2)

$$H_2CO_3 \overset{K_B}{\Leftrightarrow} HCO_3^- + H^+$$

(equation VII.3)

$$HCO_3^- \overset{K_A}{\Leftrightarrow} CO_3^{-2} + H^+$$

Where, $K_C = 1.70 \times 10^{-3}$; $K_B = 2.50 \times 10^{-4}$; $K_A = 4.68 \times 10^{-11}$.

The equations employed to arrive at these results are presented below.

(equation VII.4)

$$[CO_2] = \frac{[H^+]^2}{(1 + K_C)[H^+]^2 + K_C K_B [H^+] + K_A K_B K_C}$$

(equation VII.5)

$$[HCO_3^-] = \frac{K_B K_C [H^+]}{(1 + K_C)[H^+]^2 + K_C K_B [H^+] + K_A K_B K_C}$$

(equation VII.6)

$$[CO_3^{2-}] = \frac{K_A K_B K_C}{(1 + K_C)[H^+]^2 + K_C K_B [H^+] + K_A K_B K_C}$$

(equation VII.7)

$$[H_2CO_3] = \frac{K_C [H^+]^2}{(1 + K_C)[H^+]^2 + K_C K_B [H^+] + K_A K_B K_C}$$

VI.7. Reagent List

Table VI-18 – Brand and purity of the reagents employed in this work.

Reagent	Purity	Brand
2-Mercaptoethanol	>99%	Sigma
2,3,5-triphenyl-tetrazoliun chloride	99%	Sigma
Acetic Acid	99.8%	Sigma-Aldrich
Acrylamide/Bis Solution, 37.5:1	30%	Bio-Rad
Aluminum potassium sulfate dodecahydrate	>98%	Sigma
Ammonium chloride	99.80%	Merck
Ammonium persulfate	>98%	Sigma
Beef extract	-	Fluka
Benzyl viologen	97%	Aldrich
Biotin	>99%	Fluka
Boric acid	99%	Fluka
Brilliant blue G-250	-	Merck
Bromophenol blue	-	Merck
Calcium chloride dihydrate	99%	Fluka
Calcium pantothenate	98%	Merck
Calcium sulfate dihydrate	99%	Merck
Cobalt chloride hexahydrate	98%	Aldrich
Cobalt sulfate heptahydrate	99%	Merck
Copper chloride dihydrate	99%	Merck
Copper sulfate pentahydrate	99%	Sigma
Cyanocobalamin	99%	Roche
Di-potassium hydrogen phosphate	99%	Merck
Dimethylsulfoxid	99.9%	Aldrich
Dithiothreitol	>99%	Sigma
Ethanol	96%	Carlo Erba
Ethanol absolute anydrous	99.9%	Carlo Erba
Ferrous ammonium sulfate hexahydrate	99%	Sigma
Ferrous sulfate heptahydrate	99%	Sigma
Folin-Ciocalteu's phenol reagent	-	Merck
Glycerol	96%	Panreac
Glycine	98.5%	Panreac
Glucose	99.5%	Sigma
Hydrochloric acid	>37%	Sigma-Aldrich
Iron chloride tetrahydrate	99%	Merck
L-Ascorbic acid	99.7%	Merck
L-Cysteine	99.5%	Fluka
Magnesium chloride hexahydrate	>99%	Riedel-de Haën
Magnesium nitrate hexahydrate	99%	Merck
Magnesium sulfate	97%	Aldrich
Manganese chloride tetrahydrate	99%	Merck
Manganese sulfate monohydrate	99%	Merck
Methanol	>99.8%	Sigma
Methyl viologen	98%	Aldrich
Nicotinic Acid	98%	Sigma-Aldrich
Niquel chloride hexahydrate	98%	Merck
Nitriloacetic acid	>99%	Fluka
NZCYM broth	-	Sigma

Peptone	-	Difco
Potassium dihydrogen phosphate	99.50%	Merck
Potassium Hydroxide	87.50%	Pronalab
Potassium sodium tartrate tetrahydrate	>99%	Merck
Pyridoxine	>99.5%	Merck
Resazurin	-	BDH
Riboflavin	99%	Fluka
Sodium ascorbate	>99%	Merck
Sodium bicarbonate	99.5%	Pronalab
Sodium carbonate	99%	Merck
Sodium chloride	99.5%	Panreac
Sodium citrate dihydrate	99.5%	Sigma
Sodium dithionite	87%	Merck
Sodium DL-lactate	60%	Sigma
Sodium dodecylsulfate	>98.5%	Sigma
Sodium formate	99.5	Fluka
Sodium hydroxide	98.6%	Merck
Sodium molybdate dihydrate	99.5%	Merck
Sodium nitrate	99%	Merck
Sodium selenite pentahydrate	99%	Merck
Sodium sulfate	99%	Merck
Sodium sulfite	98%	Merck
Sulfuric acid	97%	Merck
Tetramethylethylenediamine	99%	Merck
Thiamine	>99%	Merck
Thioglycolic acid	>96.5%	Sigma
Trizma base	>99.9%	Sigma
Tryptone	-	Sigma
Yeast extract	-	Panreac
Zinc chloride	98%	Merck
Zinc granular	99%	Merck
Zinc sulfate heptahydrate	>99%	Merck